Global Biogeochemical Cycles

RESEARCH ARTICLE
10.1029/2020GB006650

Organic Carbon Export and Loss Rates in the Red Sea

Malika Kheireddine[1], Giorgio Dall'Olmo[2,3], Mustapha Ouhssain[1], George Krokos[4], Hervé Claustre[5], Catherine Schmechtig[6], Antoine Poteau[5], Peng Zhan[4], Ibrahim Hoteit[4], and Burton H. Jones[1]

[1]Red Sea Research Center (RSRC), Biological and Environmental Sciences and Engineering Division (BESE), King Abdullah University of Science and Technology (KAUST), Thuwal, Saudi Arabia, [2]Plymouth Marine Laboratory, Plymouth, UK, [3]National Centre for Earth Observation, Plymouth, UK, [4]Faculty of Earth Science and Engineering, King Abdullah University of Science and Technology (KAUST), Thuwal, Saudi Arabia, [5]Laboratoire d'Océanographie de Villefranche, Sorbonne Université, CNRS UMR 7093, Villefranche-sur-mer, France, [6]OSU Ecce-Terra, Sorbonne Université, CNRS, UMS 3455, Paris, France

Abstract The export and fate of organic carbon in the mesopelagic zone are still poorly understood and quantified due to lack of observations. We exploited data from a biogeochemical-Argo float that was deployed in the Red Sea to study how a warm and hypoxic environment can affect the fate of the organic carbon in the ocean's interior. We observed that only 10% of the particulate organic carbon (POC) exported survived at depth due to remineralization processes in the upper mesopelagic zone. We also found that POC exported was rapidly degraded in a first stage and slowly in a second one, which may be dependent on the palatability of the organic matter. We observed that apparent oxygen utilization (AOU)-based loss rates (a proxy of the remineralization of total organic matter) were significantly higher than the POC-based loss rates, likely because changes in AOU are mainly attributed to changes in dissolved organic carbon. Finally, we showed that POC- and AOU-based loss rates could be expressed as a function of temperature and oxygen concentration. These findings advance our understanding of the biological carbon pump and mesopelagic ecosystem.

Key Points:
- Only 10% of the particulate organic carbon exported survived at depth due to remineralization processes by heterotrophs
- Particulate organic carbon exported via small particles was balanced by its consumption over the seasonal cycle
- POC- and AOU-based loss rates are dependent of temperature and oxygen concentration within the mesopelagic zone

Supporting Information:
- Supporting Information S1

Correspondence to:
M. Kheireddine,
malika.kheireddine@kaust.edu.sa

Citation:
Kheireddine, M., Dall'Olmo, G., Ouhssain, M., Krokos, G., Claustre, H., Schmechtig, C., et al. (2020). Organic carbon export and loss rates in the Red Sea. *Global Biogeochemical Cycles*, *34*, e2020GB006650. https://doi.org/10.1029/2020GB006650

Received 25 APR 2020
Accepted 5 OCT 2020
Accepted article online 13 OCT 2020

1. Introduction

The ocean carbon cycle is regulated by physicochemical and biogeochemical processes collectively called carbon pumps (Boyd et al., 2019). Among these, the biological carbon pump (BCP) exports organic matter in particulate and dissolved form to the deep ocean (Boyd et al., 2019). The export of particulate organic carbon (POC) is attributed to particles sinking to depth (Boyd et al., 2019; Buesseler et al., 2007, 2020). The BCP is driven by phytoplankton cells in the euphotic layer that uptake CO_2 to produce organic carbon, which is then transported downward to the mesopelagic zone (100 to 1,000 m) through a wide range of processes (i.e., biological gravitational pump, mixed layer pump, eddy subduction pump, and vertical migration pump) (Boyd et al., 2019; Buesseler et al., 2020). The BCP is mostly responsible for the annual export of surface POC that occurs during episodic events, such as seasonal phytoplankton blooms (Honjo et al., 2014; Lutz et al., 2007). The efficiency of the BCP is usually quantified based on two main metrics: (1) the attenuation of the export flux, which is typically estimated from the exponent of a "Martin's curve fit" to the flux profile (i.e., a power law fit, Martin et al., 1987), and (2) the transfer efficiency corresponding to the fraction of POC exported in the mesopelagic zone with respect to that at the base of the euphotic zone (Buesseler et al., 2020; Llort et al., 2018).

In general, most of the organic carbon exported into the mesopelagic zone is lost due to heterotrophic remineralization processes (Cavan et al., 2017; Giering et al., 2014). Many studies revealed that remineralization of sinking organic particles is affected by local environmental conditions by either affecting particle size (fragmentation of particles) or the rate of remineralization (Lopez-Urrutia et al., 2006; Marsay et al., 2015; Martinez-Garcia et al., 2014). Under lower oxygen concentration, a larger fraction of organic carbon is thought to be unyielding to remineralization (Robinson, 2019; Weber et al., 2016). Temperature is also known to influence remineralization rates, as the heterotrophic processes responsible of the organic carbon remineralization are temperature dependent (Marsay et al., 2015; Robinson, 2019).

However, most of these studies were not performed in situ which means that changes in oxygen or temperature could have been masking other drivers. Therefore, the roles of oxygen concentration and temperature

on heterotrophic remineralization remain unclear (Laufkotter et al., 2016). A warm and/or oxygen-depleted ocean may affect the behavior of heterotrophs and thus the attenuation of organic carbon flux. Since the exported organic carbon is remineralized by heterotrophs back into inorganic carbon, oxygen and temperature changes may also impact the ocean's capacity to control the concentration of atmospheric CO_2 (Briggs et al., 2020; Kwon et al., 2009). Under a warm environment, most remineralization may occur in the upper layer of the mesopelagic zone (100–300 m), modifying how carbon and nutrients are fixed and recycled into the ocean's interior (Kwon et al., 2009). Thus, a better understanding of the processes controlling biological carbon fluxes is fundamental to predict the ocean's capacity in regulating climate change (Boyd et al., 2019; Briggs et al., 2020).

The attenuation of the flux of particles should be balanced by community processes responsible for the loss of organic carbon in the mesopelagic layer (Boyd et al., 2019; Giering et al., 2014). Several previous studies have shown that the carbon budget in the mesopelagic zone remains unbalanced (Baltar et al., 2009; Burd et al., 2010), with the notable exception of Giering et al. (2014) who were able to balance the attenuation of POC flux with the community metabolism (heterotrophic respiration). Recent studies identified additional mechanisms, such as fragmentation of particles by zooplankton, which may contribute to balancing the carbon budget in the mesopelagic zone (Briggs et al., 2020). Overall, we only have a limited knowledge of the role of the heterotrophic community in the turnover of organic matter and its responses to changes in environmental conditions (i.e., oxygen and temperature sensitivity), which compromises our predictions of carbon storage in the global ocean (Burd et al., 2010).

In the past decade, several studies demonstrated the potential of using autonomous platforms equipped with optical sensors to estimate export flux by providing particle measurements over sustained periods of time in diverse areas of the global ocean (e.g., Briggs et al., 2020; Dall'Olmo & Mork, 2014; Estapa et al., 2017, 2019). For instance, using biogeochemical-Argo (BGC-Argo) floats, estimates of carbon sequestration were improved as these provide information to track particle accumulation rates in the water column (Briggs et al., 2020).

While the Red Sea is known as a warm environment and characterized by highly stratified waters in the upper layers, its northern part behaves as a temperate ecosystem with deepening of the mixed layer depth (MLD) during winter and highly stratified waters during summer (Gittings et al., 2018, 2019). The Red Sea is the northernmost tropical sea of the global ocean and displays a strong latitudinal gradient of decreasing temperature from south (26–32°C) to north (21–28°C) (Chaidez et al., 2017; Kheireddine et al., 2017, 2018). The Red Sea has been recently identified as a fast-warming oceanic region of the global ocean, especially in its northern part (Chaidez et al., 2017). The Red Sea is also experiencing warming-related decreases in oxygen levels and hypoxic conditions in some areas of the basin (Breitburg et al., 2018; Stramma et al., 2010).

Such conditions may impact the entire Red Sea ecosystem (i.e., phytoplankton community structure, primary production, nutrient availability, temperature, and oxygen concentration), which in turn would affect the organic carbon export flux by influencing the remineralization rates of sinking particles and dissolved organic carbon (Cavan et al., 2017; Guidi et al., 2015; Marsay et al., 2015; Puigcorbe et al., 2017). Marsay et al. (2015) demonstrated a strong correlation between the Martin's exponent and the median upper 500 m water temperature for various regions of the global ocean, suggesting a strong temperature dependence of the rate of attenuation of the export flux of POC.

In this study, we examined the effect of temperature and oxygen on the remineralization of total organic carbon (TOC) and POC using measurements collected by a BGC-Argo float in the northern Red Sea. Our results suggest that remineralization processes mainly occurred within the upper layer of the mesopelagic zone and that both temperature and oxygen may control the heterotrophic respiration of the organic carbon entering the mesopelagic zone.

2. Materials and Methods

2.1. Deployment, Sampling Strategy, and Measurements

In September 2015, a biogeochemical profiling float was deployed in the northern Red Sea at 34.73°N and 27.66°E where the bathymetry is variable and shallow (<1,000-m depth) (Figure 1a). This float, identified

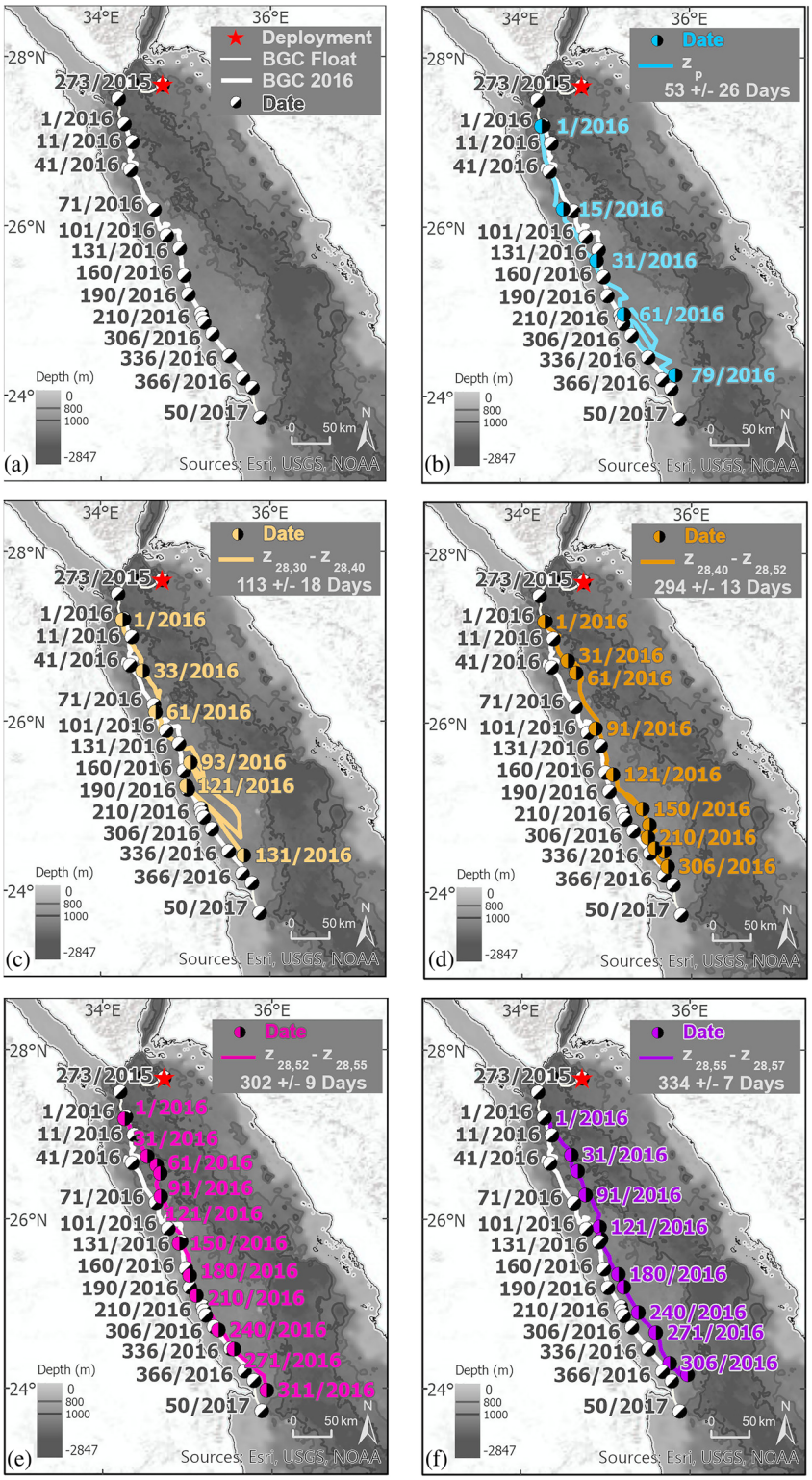

Figure 1. Trajectory of the BGC-Argo float over the period of deployment (a). The location of the deployment is indicated by the red star. The thick white line indicates the portion of the trajectory during the period of this study (1 January to 31 December 2016). The colored lines represent the average modeled trajectories of particles that were tracked within the productive layer (z_p) (b) and isopycnal layers 28.30–28.40 (c), 28.40–28.52 (d), 28.52–28.55 (e), and 28.55–28.57 kg m^{-3} (f) during the year 2016. The date (Julian day/year) is indicated on top of each trajectory. The background indicates the bathymetry along the study area.

Table 1
Summary of the Mission and Equipment for the Profiling Float Used in This Study

Float WMO#	Length of the mission	Date of deployment (dd/mm/yyyy)	Position of deployment	Date of last profile (dd/mm/yyyy)	Temporal resolution of data acquisition	Equipment
6901573	17 months	29/09/2015	33.73°N/27.66°E	19/02/2017	Daily: 29/09/2015 to 05/10/2015 5 days: 10/10/2015 to 30/10/2015 24/05/2016 to 28/07/2016 01/11/2016 to 31/12/2016 10/01/2017 to 19/02/2017 2 days: 30/10/2015 to 24/05/2016 31/12/2016 to 10/01/2017 10 days: 28/07/2016 to 01/11/2016	CTD (Seabird SBE 41CP) Radiometry (Satlantic OCR) WET Labs ECO Puck Triplet Oxygen sensor (Aanderaa optode, model 4330)

from its World Meteorological Organization number 6901573 (http://argo.jcommops.org), acquired vertical profiles of bio-optical and biogeochemical variables as well as temperature and salinity measurements. The mission parameters and equipment of the float are summarized in Table 1 and its trajectory is displayed in Figure 1a. The maximum parking depth was set to 1,000 m. The float was programmed to surface at noon every 2, 5, or 10 days depending on the season. Data acquisition was nominally at 10-m resolution between 250 and 1,000 m of depth, 1-m resolution between 10 and 250 m, and increased to 0.20-m resolution between 10 m and the surface (Organelli et al., 2017). Float data were downloaded from the global Argo database (ftp://ftp.ifremer.fr/ifremer/argo/).

Vertical profiles of chlorophyll-a (chla) fluorescence and the volume scattering function (measured at 124° and at 700 nm) were obtained using a Wet Labs ECO sensor. The photosynthetically available radiation (PAR, see acronym definitions in Table 2) was measured with a Satlantic OCR radiometer. Raw counts for each parameter were transformed into geophysical quantities by applying the manufacturer-provided scaling factor and dark count. Then, as recommended by the Argo data management procedures (Wong et al., 2015), each profile was quality controlled by applying methods that have been specifically developed for each variable (Organelli et al., 2017; Thierry, Bittig, Gilbert et al., 2018; Thierry, Bittig, & The Argo-Bgc Team, 2018, and references therein). Dissolved oxygen concentrations (O_2) were determined using an Aanderaa optode sensor (model 4330).

Following Schmechtig et al. (2015), vertical profiles of chla concentration (mg m^{-3}) were adjusted for non-zero deep values and corrected for non-photochemical quenching according to Xing et al. (2018). The chla values were further divided by a factor of 2 to correct for the overestimation observed by standard

Table 2
Symbols of Variables Used in This Study With Their Definitions and Units

Symbol	Definition	Unit
POC	Particulate organic carbon	mg m^{-3}
chla	Chlorophyll a fluorescence	mg m^{-3}
b_{bp}	Particulate backscattering coefficient	m^{-1}
PAR	Photosynthetically available radiation	µmol quanta m^{-2} s^{-1}
MLD	Mixed layer depth	m
z_p	Productive layer	m
E_{z_p}	Net POC flux just below z_p	mmol POC m^{-2} y^{-1}
E_{z_i}	Seasonal net POC export rate	mmol POC m^{-2} y^{-1}
b	Martin's exponent	Dimensionless
T_{z_i}	Transfer efficiency	Dimensionless
$E_{z_{iF}}$	Net fast maximum (instantaneous) carbon export	mmol POC m^{-2} d^{-1}
$L_{z_{iF}}$	Net fast POC loss rates	mmol POC m^{-2} d^{-1}
$L_{z_{iS}}$	Net slow POC loss rates	mmol POC m^{-2} d^{-1}
$L_{z_{iF}}$*	Fast POC-specific loss rates	y^{-1}
$L_{z_{iS}}$*	Slow POC-specific loss rates	y^{-1}
$L_{z_i}^{AOU}$	Net TOC loss rates	mol C m^{-2} d^{-1}

Wet Labs fluorometers as described in Roesler et al. (2017). The particulate backscattering coefficient at 700 nm (b_{bp} (700) in m^{-1}) was calculated as described in Schmechtig et al. (2016). First, the particulate volume scattering function was calculated by removing the contribution of pure seawater that depends on both temperature and salinity (Zhang et al., 2009). Then, the particulate volume scattering function was converted into b_{bp} as recommended in Boss and Pegau (2001) and Sullivan et al. (2013). Spikes were removed from the chla and b_{bp} measurements as described in Briggs et al. (2011). The PAR vertical profiles acquired during unstable sky and sea conditions as well as during sporadic atmospheric clouds were discarded following Organelli et al. (2016). Then, the remaining PAR profiles with non-zero dark measurements at depth and wave focusing in the upper part of the profiles were removed (Zaneveld et al., 2001). O_2 measurements were processed by applying a locally derived factor (~1.06) to each profile based on the comparison between the float's percent oxygen saturation (O_2sat) values and those from the monthly World Ocean Atlas climatology (WOA09) (Figure S1), as described by Takeshita et al. (2013). Finally, quality-controlled vertical profiles of chla, b_{bp}, PAR, and O_2 were binned in 1-m intervals and used for the analyses in this study.

Apparent oxygen utilization (AOU) was computed as the difference between O_2 and the oxygen concentration at saturation (O_2sat) following the method of Garcia and Gordon (1992). Then, positive changes in AOU were converted to changes in TOC using the molar ratio $\Delta C{:}\Delta O_2 = 0.688$ (Anderson & Sarmiento, 1994).

The MLD was calculated as the depth at which density exceeded the density at 10 m by 0.03 kg m^{-3} (de Boyer Montegut et al., 2004). The euphotic depth was calculated as the depth at which PAR was 1% of its surface value (Morel & Berthon, 1989) which corresponded to the depth below which less than 5% of chlorophyll-containing particles were detected. Finally, the bottom of the productive layer (z_p), defined as the region where particles can be produced by photosynthesis, was computed as the maximum between the euphotic depth and the MLD.

2.2. From b_{bp} and AOU to Organic Carbon Stocks and Fluxes

Particle backscattering is sensitive to the presence of particles in the size range 0.2–20 μm in general (Stramski et al., 2004) and more specifically between 1 and 10 μm within the surface of oligotrophic waters (Organelli et al., 2018). In this study, b_{bp} was used to estimate the concentration of POC using an empirical relationship ($[POC] = 40{,}233\ b_{bp} - 11$) established for Red Sea waters based on in situ measurements collected during different cruises performed between 2014 and 2016. The slope of this relationship was within the range of those reported in previous studies (Cetinic et al., 2012; Rasse et al., 2017; Stramski et al., 2008). Details about the POC versus b_{bp} (700) relationship are provided in the supporting information.

To compute stocks and net rates of POC accumulation within homogeneous water masses, density measurements were used to define different layers within the mesopelagic zone. To verify the homogeneity of these layers along the trajectory of the float, the spiciness metric was calculated according to Flament (2002). This variable allowed us to identify changes in water masses with distinct thermohaline properties but having similar density and thus to ensure spatial and temporal homogeneity within the chosen isopycnal layers. The float remained in nearly homogeneous water masses only during the year 2016 (see supporting information), and thus, only data from this year are further considered in this study. Because the float moved significantly over the period of the analysis (Figure 1a), Lagrangian particle tracking, based on previously validated model results, was used to further test the extent to which the float sampled homogeneous water masses during the analysis period. Essential information regarding the modeling study is described in the supporting information. Briefly, the general (1 km) circulation in the Red Sea was simulated based on a three-dimensional high-resolution MIT general circulation model (MITgcm) (Marshall et al., 1997) configured for the Red Sea (Yao et al., 2014a, 2014b). The trajectories of numerous passive particles from a point-source region corresponding to the float location were then simulated and tracked using the connectivity modeling system (CMS) (Paris et al., 2013).

POC values were integrated over the productive layer and over different isopycnal depths (28.30 to 28.57 kg m^{-3}) below the productive zone (Dall'Olmo & Mork, 2014): (1) from the surface (z_0) to isopycnal depth 28.57 kg m^{-3} ($z_{28.57}$) ($z_0 - z_{28.57}$, $iPOC_0^{28.57}$) corresponding to the whole water column (excluding bottom effects), (2) within the productive layer ($z_0 - z_p$, $iPOC_0^{z_p}$), (3) within the entire mesopelagic layer defined as the isopycnal layer 28.30–28.57 kg m^{-3} ($z_{28.30} - z_{28.57}$, $iPOC_{28.3}^{28.57}$), and (4) over gradually deeper isopycnal

layers of the mesopelagic zone ($iPOC^{28.57}_{28.30+z_i}$, with z_i = 0.1, 0.22, 0.25, and 0.27 kg m^{-3} isopycnals). The different isopycnal layers were chosen based on their physical properties and the vertical resolution of the float in order to have enough data points to integrate POC values over gradually deeper layers of the mesopelagic zone. We paid particular attention to exclude sediment resuspended from the bottom from the analysis to avoid interpreting these resuspensions as POC fluxes.

The net POC flux (E) within the isopycnal layers 28.30 + z_i was then estimated from the rate at which POC stocks in the different layers of the mesopelagic ($iPOC^{28.57}_{28.30+z_i}$) varied as a function of time, and E_{z_p} represents the net POC flux just below the productive layer (Dall'Olmo & Mork, 2014). As the float did not sample at high vertical and temporal resolution, it was not possible to extract information about sinking of large particles in the mesopelagic layer (Briggs et al., 2020). Thus, the potential export of large particles/aggregates was not considered in this study. Our estimates of POC fluxes are mainly attributed to small slowly sinking particles, given that de-spiked b_{bp} measurements are not expected to be sensitive to large particles (Briggs et al., 2011).

The vertical variation of E was then used to estimate the so-called Martin's exponent, b, using the power law function, $E_z = E_{z_p}\left(z/z_p\right)^b$ (Martin et al., 1987). While this model remains debated (Guidi et al., 2015; Marsay et al., 2015), estimates of the b exponent allow us to compare the results from our study with other previously studied regions of the global ocean. The fraction of surface POC flux exported to the different layers of the mesopelagic zone, T_{z_i} (transfer efficiency), was computed as the ratio E_{z_i}/E_{z_p} (Buesseler & Boyd, 2009).

The seasonal net export rate in the mesopelagic layers (E_{z_i}) was also estimated by fitting a linear least-squared model from the time when $iPOC^{28.57}_{28.3}$ was minimal (late January) to the time when $iPOC^{28.57}_{28.3}$ reached its maximum value (late February). The fast maximum (instantaneous) net carbon export, $E_{z_{iF}}$, within the mesopelagic zone was determined from the slope of the straight line fitted by a linear least-squared model over the time period of fast POC export (late February, about 6 days).

Removal of POC occurred in two stages. The first stage was observed during a short period of time qualified as "fast removal" and the second was observed over a longer period of time qualified as "slow removal." Thus, carbon fast and slow net loss rates, $L_{z_{iF}}$ and $L_{z_{iS}}$, respectively, were estimated as the time rate of change of POC stocks (linear fit), when POC stocks within a given layer of the water column were observed to decline for each stage. Fast losses occurred in early March (for about 6 days), while slow ones occurred from March to September (about 205 days). Fast and slow carbon-specific loss rates, $L_{z_{iF}}$* and $L_{z_{iS}}$*, respectively, were computed by dividing $L_{z_{iF}}$ or $L_{z_{iS}}$ by the average POC stocks during the period of removal. Finally, the loss rates in TOC (derived from AOU), $L^{AOU}_{z_i}$, were estimated as the time rate of change of AOU (linear least-square fit) from early March (minimum of the average of AOU) to early June (maximum of the average of AOU) within a given layer of the water column.

3. Results

3.1. Physical Characteristics Along the Float Trajectory

All particles released in the model at the location of the float on 1 January 2016 (34.27°N and 27.20°E) within the productive layer and the four gradually deeper isopycnal layers of the mesopelagic zone followed the western boundary currents along the African coast up to a latitude of 24°N. Their average trajectories within each layer are presented in Figures 1b–1f and agree reasonably well with the float's trajectory. They generally exhibited low dispersion in their pathway. The mean transport velocities and the related drift times were related to the initial release depth. Specifically, particles in the productive layer (145 ± 37 m) needed 53 ± 26 days to reach the position of the float at the end of the period considered in the analysis (Figure 1b), whereas this time increased to 113 ± 18 days at 180 ± 43 m depth (Figure 1c) and to 334 ± 7 days for those released deeper (300–485 m) (Figure 1f). Even if the surface particles traveled faster than the float, this is not a major problem for our study because particles were injected into the mesopelagic from the surface layer only during a localized event (late February 2016). Furthermore, the rest of the dynamics we analyzed occurred in the mesopelagic zone, where the float followed water masses in a quasi-Lagrangian fashion.

Table 3
Average and Standard Deviation of Spiciness Metric Over Gradual Isopycnal Layers of the Mesopelagic Zone

	$z_{28.30} - z_{28.40}$	$z_{28.40} - z_{28.52}$	$z_{28.52} - z_{28.55}$	$z_{28.55} - z_{28.57}$
Average ± standard deviation	7.986 ± 0.006	7.963 ± 0.008	7.918 ± 0.005	7.906 ± 0.003

Temperature-salinity diagrams produced from the Conductivity-Temperature-Depth (CTD) measurements collected along the float trajectory, as well as a compilation of historical stations (see supporting information) collected in the Red Sea, are presented in Figure S4. Different water masses were identified with distinct physical and chemical characteristics: the Red Sea surface water (RSSW), the Red Sea outflow water (RSOW), and the Red Sea deep water (RSDW; Sofianos & Johns, 2007). The RSSW mass corresponds to the surface waters and is characterized by relatively high variability in salinity. On the other hand, the RSOW and the RSDW are deeper water masses characterized by constant temperature and salinity.

Each of the four mesopelagic layers studied was characterized by temperatures and salinities that corresponded to the RSOW and RSDW masses (Figures S4 and S5). During 2016, the four isopycnal layers sampled in mesopelagic zone exhibited fairly stable temperatures (22.15°C ± 0.10°C; 21.85°C ± 0.09°C; 21.68°C ± 0.05°C; and 21.63°C ± 0.04°C, respectively) and salinities (40.47 ± 0.05; 40.52 ± 0.03; 40.53 ± 0.01; and 40.53 ± 0.01, respectively) along the float trajectory (Figure S5). In addition, the spiciness metric was used to reveal the underlying isopycnal mixing that could alter the variability of biogeochemical properties on the same isopycnal layers (Figure S6). We found that each of the four mesopelagic layers was also characterized by low spiciness variability (Table 3), whereas high spiciness variability was observed in response to unstable vertical salinity and temperature gradient immediately near the surface layer (Figure S6).

3.2. Temporal Evolution of chla and b_{bp} Vertical Distribution

The seasonal dynamics of chla and b_{bp} are displayed in Figure 2. In the upper productive layer, chla and b_{bp} exhibited a similar seasonal pattern with highest values during winter and lower values during the rest of the year. These concomitant high chla and b_{bp} values within the surface layer were associated with an increase

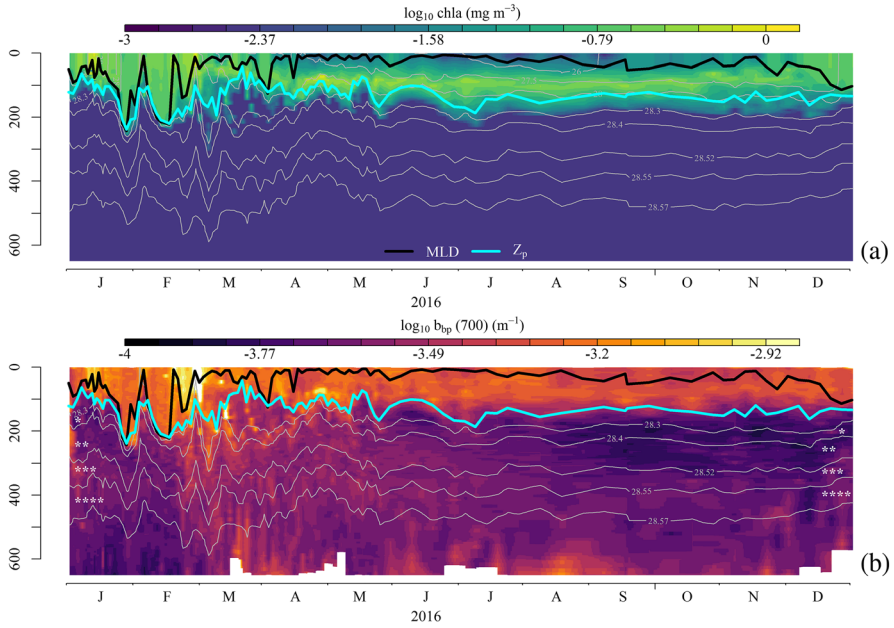

Figure 2. Time series of the vertical distributions of chla (a) and b_{bp} (b) for the float data collected by the float in 2016. Gray lines are the isopycnals 28.3, 28.4, 28.52, 28.55, and 28.57 kg m^{-3}. The chla and b_{bp} (700) are plotted on a logarithmic scale. The black and cyan lines represent the mixed layer depth (MLD) and the productive layer (z_p), respectively. The symbols *, **, ***, and **** represent the isopycnal layers used in the rest of the analysis: 28.30–28.40, 28.40–28.52, 28.52–28.55, and 28.55–28.57 kg m^{-3}, respectively.

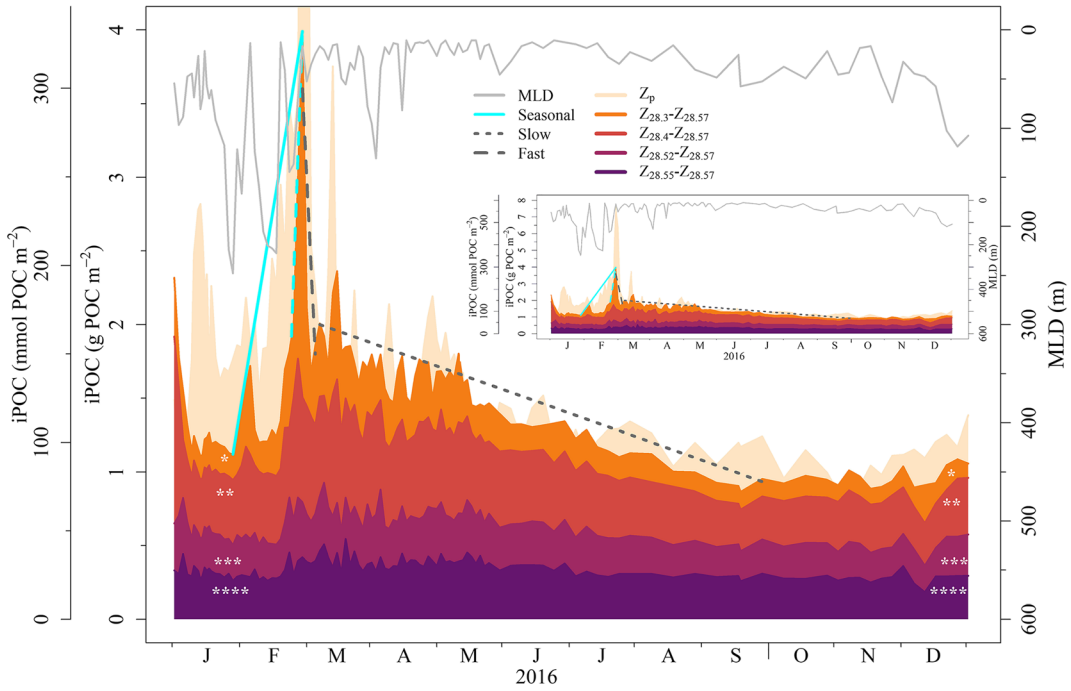

Figure 3. Vertically integrated POC stocks ($iPOC^{Z_{28.57}}_{Z_{28.30}+Z_i}$) estimated from the float data during 2016 within the productive zone and the mesopelagic zone: the isopycnal layer 28.30–28.57 kg m^{-3} representing the entire mesopelagic layer and progressively deeper isopycnal layers ($iPOC^{Z_{28.57}}_{Z_{28.30}+Z_i}$, with Z_i = 0.1, 0.22, 0.25, and 0.27 kg m^{-3}). The symbols *, **, ***, and **** refer to the same isopycnal layers presented in Figure 4. Cyan solid and dashed lines: linear regressions used to estimate seasonal and daily fast carbon export rate, E_{Z_i} and $E_{Z_{iF}}$, respectively. Gray dashed and dotted lines: linear regressions used to estimate daily fast and slow carbon loss rates, $L_{Z_{iF}}$ and $L_{Z_{iS}}$, respectively.

of phytoplankton biomass following the deepening of the MLD (Figure 2). In the summer stratified period, chla showed a pronounced deep chlorophyll maximum DCM (Figure 2a).

3.3. Export Fluxes and Transfer Efficiency

After the phytoplankton biomass increased in the productive layer, the POC stock in the mesopelagic zone ($iPOC^{28.57}_{28.3}$) increased to its maximum value (~333 mmol POC m^{-2}, Figure 3). About 7 days later, this POC stock decreased by about 166 mmol POC m^{-2}. Then, over the spring–summer seasons, a slow decline of the stock was observed that amounted to around 83 mmol POC m^{-2}.

The seasonal net carbon export flux below the productive layer, E_{Z_p}, was 233 ± 46 mmol POC m^{-2} y^{-1} and was mainly associated with a fast export event (25.8 ± 5.2 mmol POC m^{-2} d^{-1}) that occurred just after the summer stratification was established (Figure 3). Vertically resolved seasonal and fast values of carbon export below the productive layer, E_{Z_i} and $E_{Z_{iF}}$, respectively, decreased exponentially as a function of depth (Figures 4a and 4b). Most of the POC was degraded in the upper part of the mesopelagic layer (about 72% between 72- and 157-m depth), while less than 10% of the POC reached the bottom of the mesopelagic zone (Figure 4c).

The seasonal estimates of POC flux were fitted to the equation of Martin et al. (1987) to determine the exponent of the attenuation flux, b, which had a mean (±standard deviation) value of 1.53 ± 0.16.

3.4. Oxygen-Based Respiration Rates

The AOU inventory exhibited a ventilation-respiration cycle (Figure 5). When the mixed layer reached its maximum depth in January–February, the AOU inventory was ventilated. During this mixing period, ephemeral restratifications were observed that caused an anomalous rise in the average AOU values, but these were excluded from the rest of the analysis. During the period of stratification, the AOU inventory increased by 7% to 55% throughout the winter spring until the end of spring (early June). Then, over the summer, the inventory in AOU remained relatively stable and increased again from October.

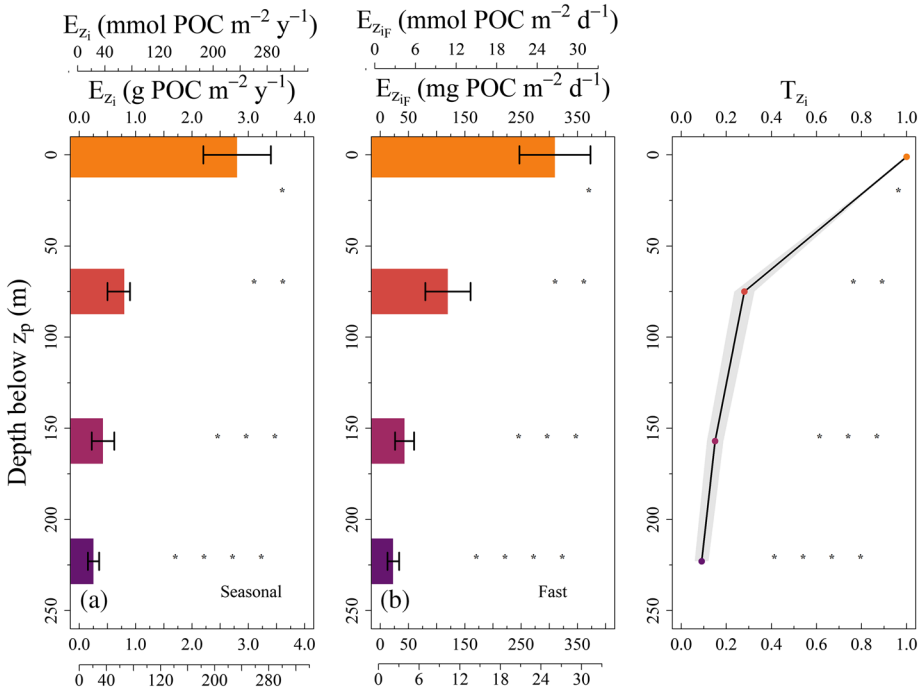

Figure 4. Estimates of seasonal and fast export rates E_{Z_i} (a) and $E_{Z_{iF}}$ (b) and transfer efficiency (T_{Z_i}) (c) over the analyzed isopycnal layers of the mesopelagic zone. Error bars represent one standard deviation. The line in plot (c) represent T_{Z_i} and the gray area its standard deviation. The symbols *, **, ***, and **** refer to the isopycnal layers 28.30–28.40, 28.40–28.52, 28.52–28.55, and 28.55–28.57 kg m^{-3}, respectively (see also Figure 2).

3.5. Organic Carbon Losses

In early March, the POC stock just below the productive layer decreased approximately from 333 to 166 mmol POC m^{-2} in about 7 days (Figure 3), corresponding to a fast POC loss rate $L_{Z_{pF}}$ of 24 ± 6 mmol POC m^{-2} d^{-1}. POC stocks decreased further by around a factor of 2 over the spring–summer (~205 days), corresponding to a

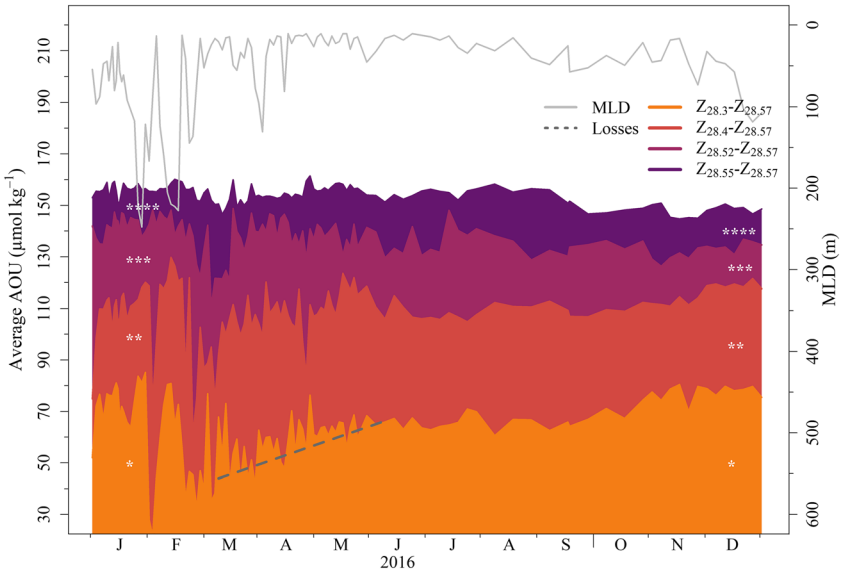

Figure 5. Vertically averaged AOU estimated from the float data during 2016 within each isopycnal layer of the mesopelagic zone. The symbols *, **, ***, and **** refer to the same isopycnal layers presented in Figure 4. Gray dashed lines: linear regression used to estimate daily carbon loss rates, $L_{Z_i}^{AOU}$.

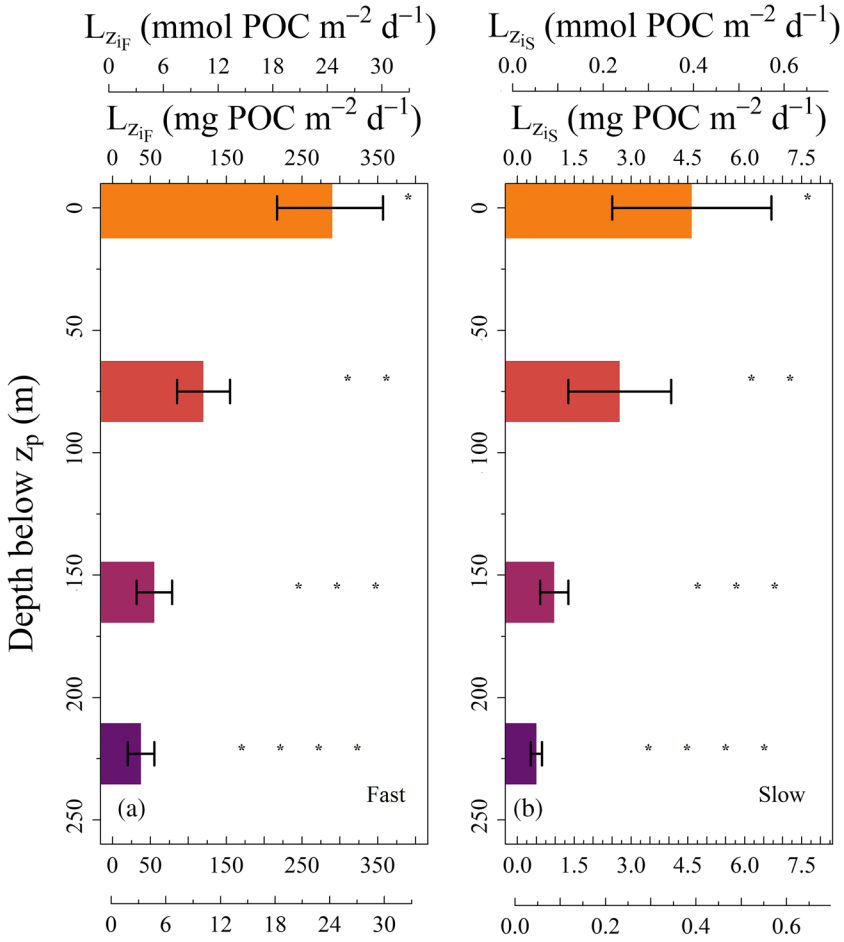

Figure 6. Fast and slow loss rates $L_{z_{iF}}$ (a) and $L_{z_{iS}}$ (b) over gradually deeper isopycnal layers of the mesopelagic zone. Error bars represent one standard deviation. The symbols *, **, ***, and **** refer to the isopycnal layers 28.30–28.40, 28.40–28.52, 28.52–28.55, and 28.55–28.57 kg m^{-3}, respectively (see also Figure 4).

slow loss rate $L_{z_{pS}}$ of 0.41 ± 0.16 mmol POC m^{-2} d^{-1} (Figure 3). As observed for E_{z_i} and $E_{z_{iF}}$, $L_{z_{iF}}$ and $L_{z_{iS}}$ also decreased exponentially as a function of depth (Figures 6a and 6b and Table 4). Average AOU just below the productive layer increased from ~44 to ~66 μmol kg^{-1} until the end of the spring season (~92 days), corresponding to a loss of TOC at a rate, $L_{z_p}^{AOU}$, of 1 ± 0.25 mol C m^{-2} y^{-1} (10.8 ± 2.7 mmol C m^{-2} d^{-1}). $L_{z_i}^{AOU}$ also decreased exponentially as a function of depth (Table 4).

4. Discussion

4.1. Assumption of Spatial Homogeneity

The model-based Lagrangian particle tracking suggested that deep mesopelagic waters moved approximately at the same speed as the float, while surface waters moved faster than the float (Figure 1). This

Table 4
Average and Standard Deviation of Net Carbon Export and Loss Rates Over Gradual Isopycnal Layers of the Mesopelagic Zone

	$L_{z_{iF}}$ (mmol POC m^{-2} d^{-1})	$L_{z_{iS}}$ (mmol POC m^{-2} d^{-1})	$L_{z_i}^{AOU}$ (mmol C m^{-2} d^{-1})
$z_{28.30} - z_{28.40}$	24 ± 6	0.41 ± 0.16	10.8 ± 2.7
$z_{28.40} - z_{28.52}$	10 ± 3	0.23 ± 0.12	9.1 ± 2.2
$z_{28.52} - z_{28.55}$	4.6 ± 1.9	0.08 ± 0.03	5.4 ± 1.2
$z_{28.55} - z_{28.57}$	2.3 ± 1.4	0.042 ± 0.013	2.8 ± 0.7

suggests that the float followed in a quasi-Lagrangian manner the same mesopelagic water masses during the analysis period. This conclusion is further supported by the spatiotemporally coherent physical characteristics (temperature, salinity, and spiciness) that we observed within each layer of the mesopelagic zone. Overall, these results support our use of the float data as a time series.

4.2. Small Particle Dynamics

Large post-bloom sinking organic aggregates were likely fragmented by biological and/or physical mechanisms (Burd & Jackson, 2009) and generated the small particles we observed in this study. These small slowly sinking particles are expected to be mostly remineralized by heterotrophic bacteria in the mesopelagic zone (Goutx et al., 2007; Herndl & Reinthaler, 2013), because only low concentrations of zooplankton can be found in the Red Sea mesopelagic waters (Dypvik & Kaartvedt, 2013). In addition, bacterial activities, including remineralization rates, are enhanced by warm environments as the Red Sea (Lopez-Urrutia et al., 2006; Sarmento et al., 2010).

4.3. POC Fluxes and Transfer Efficiency

We observed that about only 10% of the material exported reached depths greater than 220 m (Figure 4c). This suggests that most of the particulate matter was relatively labile and was remineralized in the upper mesopelagic zone, which is consistent with the relatively high value of Martin's *b* exponent we estimated. Marsay et al. (2015) found a *b* value of 1.59 in the North Atlantic subtropical gyre and hypothesized that a strong attenuation of the flux may occur in the upper mesopelagic in warm waters due to strong recycling of organic material by heterotrophic respiration. In our study, the high value of 1.53 ± 0.16 suggests that strong remineralization processes occurred in the upper layer of the mesopelagic zone, possibly as a response to the high temperature of the Red Sea.

4.4. Organic Carbon Losses

To the best of our knowledge, this study presents the first seasonal estimates of fast and slow net POC loss rates from small slowly sinking particles in the mesopelagic zone. Losses of POC through the mesopelagic zone are mainly attributed to remineralization by bacteria (Herndl & Reinthaler, 2013; Robinson et al., 2010). However, the temporal and spatial variability of bacterial remineralization rates in the mesopelagic zone still needs to be quantified accurately and leads to uncertainties in the mesopelagic carbon budget (Giering et al., 2014). The contribution of small slowly sinking particles could be a potential supplementary carbon source capable of balancing carbon budgets in the mesopelagic zone (Boyd et al., 2019; Giering et al., 2014). Thus, our estimates of net POC loss rates from small particles could be used to further constrain the mesopelagic carbon budget as well as to parameterize biogeochemical models.

Our AOU-based remineralization rates (1.00 ± 0.25 mol C m^{-2} y^{-1}) are within the range of values of organic carbon remineralization rates previously reported in the Red Sea (1.25 ± 0.70 mol C m^{-2} y^{-1}; Calleja et al., 2019) and in other oceanic regions (0.7 to 3.6 mol C m^{-2} y^{-1}) using similar or different techniques (AOU, oxygen, leucine incorporation, Dissolved Organic Carbon [DOC] measurements) (Devries & Weber, 2017; Feely et al., 2004; Giering et al., 2014; Robinson, 2019, and references therein).

Our oxygen-based remineralization rates are significantly higher (25-fold) than our POC-based loss rates. These differences likely arise because changes in AOU integrate processes and carbon stocks that we cannot detect with b_{bp}. Also, they could be due to differences observed in the timing between POC and AOU losses which may be due to variability and sensitivity of the carbon pool (type and stoichiometry). Among these additional carbon stocks detected by AOU, but not b_{bp}, the most important is the pool of dissolved organic carbon that is known to support most (50–90%) of the remineralization (Abell et al., 2000; Hansell & Carlson, 2001). In agreement with these previous studies, we found that slow-sinking POC could account for less than 10% of the overall organic matter remineralization recorded by losses in oxygen. Recently, Torfstein et al. (2020) observed high POC flux values (1.7 to 4.6 mol C m^{-2} y^{-1}) within the mesopelagic layer in the Gulf of Aqaba in the Red Sea which suggest that a large fraction of POC flux attributed to large fast-sinking particles (>10 μm) might not be detected here. The remaining part of these losses should thus be assigned to the consumption of DOC and larger particles (>10 μm).

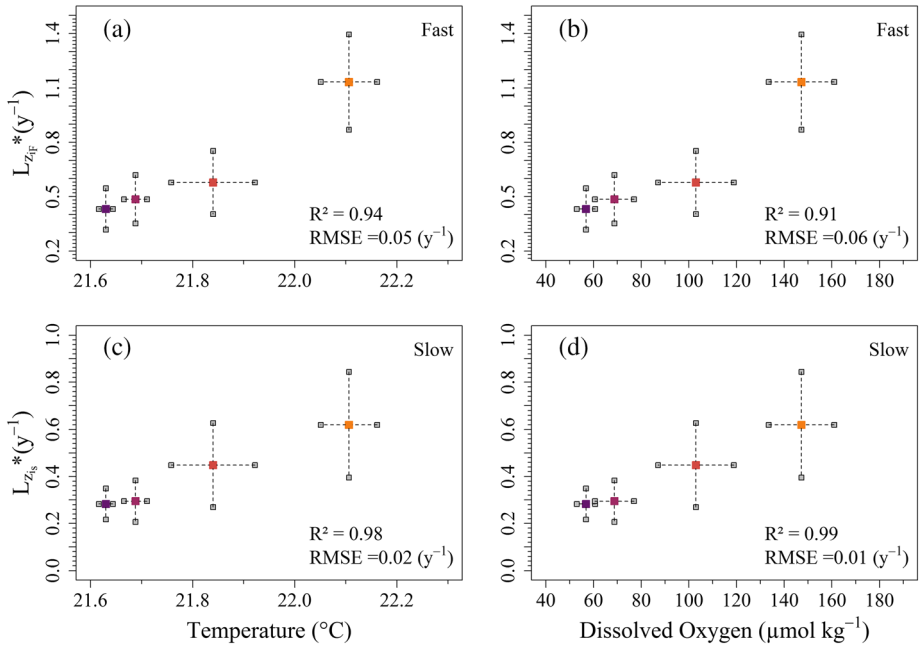

Figure 7. POC-specific (fast and slow) loss rates as a function of the mean temperature (a, c) and oxygen concentration (b, d) over gradually deeper isopycnal layers of the mesopelagic zone. Error bars represent one standard deviation.

4.5. Drivers of Organic Carbon Loss

Our estimated POC- and AOU-based loss rates decreased with depth, which could be due to multiple factors that also decrease as a function of depth. These depth-dependent factors include (1) the concentration of POC and DOC that are the substrates for remineralization; (2) the lability of carbon (e.g., their composition, Roder et al., 2013); and (3) temperature and oxygen concentration (Robinson, 2019, and references therein) that affect microbial rates. To attempt to explain the variability of our loss rates with depth (~65% of variation), we computed POC-specific loss rates (rates per unit POC stock). Unfortunately, we do not have in situ measurements of TOC, so we could not normalize the AOU-based loss rates. The POC-specific loss rates still varied over a significant range (~40% of variation), suggesting that the POC variability with depth could not explain all the observed variations in the organic carbon loss rates. In other words, the variability in loss rates with depths could not be explained entirely by a decrease in the available substrates.

We then investigated the variability of POC-specific and AOU-based loss rates as function of temperature (Brewer & Peltzer, 2017; Figures 7 and 8). POC-specific loss rates and AOU-based loss rates were significantly correlated with temperature, despite the relatively narrow range of temperatures observed ($[L_{z_{iF}}* = 1.47T - 31.5]$, $R^2 = 0.94$, Figure 7a; $[L_{z_{iS}}* = 0.74T - 15.7]$, $R^2 = 0.98$, Figure 7c; $[L_{z_i}^{AOU} = 17.5T - 373]$, $R^2 = 0.88$, Figure 8a; $N = 4$, $p < 0.01$).

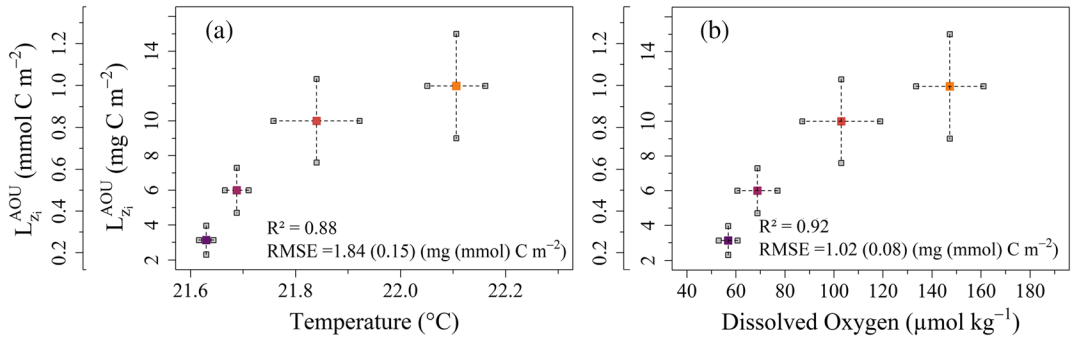

Figure 8. AOU-based loss rates as a function of the mean temperature (a) and oxygen concentration (b) over gradual isopycnal layers of the mesopelagic zone. Error bars represent one standard deviation.

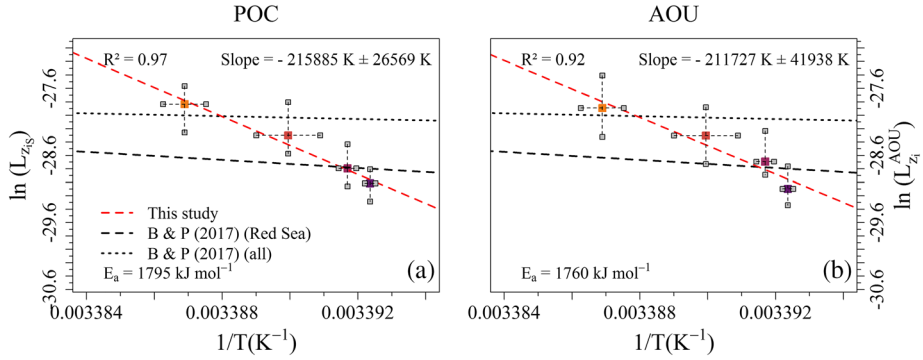

Figure 9. Arrhenius activation energy plots for $L_{z_{iS}}$ (a) and $L_{z_i}^{AOU}$ (b) over gradual isopycnal layers of the mesopelagic zone. Error bars represent one standard deviation.

Using the Arrhenius law (Arrhenius, 1889), we estimated the activation energy (E_a) from the slope of a plot of the natural logarithm of the change in the AOU or POC averaged at each time step within a given isopycnal layer of the mesopelagic zone versus the inverse absolute temperature in Kelvin (1/T) (Figure 9, Brewer & Peltzer, 2017). The activation energy is expected to be inversely related to the lability of the substrate of a chemical reaction (in this case, the remineralization of organic matter): the more a compound is recalcitrant, the higher is E_a. Furthermore, E_a can vary as a function of the organisms degrading the organic matter (Davidson et al., 2000; Davidson & Janssens, 2006). No significant differences between E_a reported for POC and TOC loss rates were found (Figure 9).

However, we found higher E_a values (>1,760 kJ mol^{-1}) compared to those reported for other regions of the global ocean (60.8–758.1 kJ mol^{-1}) as well as the Red Sea (392.5 kJ mol^{-1}), even though our carbon loss rates are within the same range than those reported for the Red Sea by Brewer and Peltzer (2017) (Figure S7).

Our estimates of E_a are, however, similar to those reported for the eastern part of the Mediterranean Sea (1,663 kJ mol^{-1}, Brewer & Peltzer, 2017). These authors suggested that their Mediterranean site had experienced a full column overturn and thus suspected that their data set was not in a steady-state condition due to a deep mixing event, which could explain the high E_a value obtained. Our analyses of the stability of the water column (Figure S6 and Table 3) indicate that this was not the case for our study. Thus, our relatively high E_a values are consistent with slow remineralization of relatively recalcitrant organic matter and/or might be an artifact of the very narrow range in temperature observed in our study. Alternative explanations for the differences in E_a observed between our study and that of Brewer and Peltzer (2017) could be that our loss rates were (1) estimated using different techniques and (2) estimated within the northern Red Sea compared to the whole basin in Brewer and Peltzer (2017). Indeed, the data used for the Red Sea in Brewer and Peltzer (2017) are based on AOU measurements, which were collected during spring and fall seasons along the central axis from south to north. Further investigations are needed to explain these differences in activation energies.

Although it is tempting to interpret the strong correlations between loss rates and temperature presented in Figures 7 and 8 as causal links, the real driving factors of the variability in L_{z_i}* and $L_{z_i}^{AOU}$ could covary with and thus be confounded by oxygen. Indeed, POC-specific loss rates were also strongly correlated with oxygen, which varied over a wider range than temperature ($[L_{z_{iF}}* = 0.008O_2 - 0.06]$, $R^2 = 0.91$, Figure 7b; $[L_{z_{iS}}* = 0.004O_2 + 0.05]$, $R^2 = 0.98$, Figure 7d; $N = 4$, $p < 0.01$). We also found a robust correlation between AOU-based loss rates and oxygen ($[L_{z_i}^{AOU} = 0.094O_2 - 1.02]$, $R^2 = 0.92$, Figure 8b; $N = 4$, $p < 0.01$). While oxygen was strongly correlated with temperature (Figure S8), given the greater dynamic range of oxygen with respect to temperature, we have more confidence in relating oxygen than temperature with organic carbon losses rates as a function of depth. This is consistent with previous studies that observed remineralization processes taking place mainly in the upper layer of the mesopelagic zone and slower remineralization rates under lower oxygen concentration (Laufkotter et al., 2017; Le Moigne et al., 2017; Robinson, 2019). Based on these observations, we surmise that temperature and oxygen might be key parameters controlling the respiration of the organic carbon pool entering the mesopelagic zone by heterotrophic organisms. Hence,

the sensitivity of heterotrophic organisms to variations in ocean temperature and oxygen concentration may have implications for controlling concentration of atmospheric CO_2 and thus regulating the climate.

Although oxygen was strongly related to carbon loss rates, the stoichiometry of organic matter could also explain the variability observed in loss rates. The C:N ratio of organic matter increases with depth in the Red Sea (Calleja et al., 2019; Roder et al., 2013), indicating that organic matter becomes more recalcitrant at depth (Paulmier et al., 2009; Thomas, 2002). As consequence, we would expect lower remineralization rates deeper in the water column. Unfortunately, we do not have coincident particulate or dissolved organic nitrogen measurements to test this hypothesis.

4.6. Why Are There Fast and Slow Net POC Loss Rates From Small Slowly Sinking Particles?

Small slowly sinking particles (<10 μm) can be degraded rapidly by mesozooplankton and bacteria, or degraded slowly (weeks to months) by bacteria (Goutx et al., 2007; Sempere et al., 2000). Our results showed that more than 85% of the POC exported to the mesopelagic was degraded within a few days, while the remaining portion of POC (less than 15%) was degraded over the course of weeks to months. We also showed that the fast loss of POC occurred at temperatures similar to those measured during the slow decline. Thus, we can infer that the observed differences in fast and slow loss rates are not due to temperature, but most likely to variations in the organisms consuming the carbon (e.g., zooplankton and bacteria) within the mesopelagic zone (Calleja et al., 2018) and/or to changes in the lability of the POC. In other words, we may have observed slow loss rates of POC over the spring–summer seasons, because after the recorded fast losses, the remaining small particles might have become less nutritious and thus less palatable for bacteria. Moreover, the bacteria and zooplankton communities consuming particles during the periods of fast and slow loss rates might have been different.

4.7. Mesopelagic Carbon Budget

Closing the mesopelagic carbon budget has been challenging due to the complexity of the mesopelagic food web and the numerous processes involved in the export and remineralization of organic carbon. Numerous studies have found a strong imbalance in the mesopelagic zone by up to an order of magnitude between heterotrophic carbon demand and the flux of sinking carbon (Anderson & Ryabchenko, 2009; Burd et al., 2010; Steinberg et al., 2008). We found that the POC exported via small particles was balanced by its consumption (sum of the fast and slow small particle POC losses) over the seasonal cycle (Figure S9). Our results regarding export and losses of POC are consistent with the findings of Giering et al. (2014) for the Northeast Atlantic Ocean, where they suggest that the main role of zooplankton is to fragment aggregates into smaller particles that are easily degradable by prokaryotes. Recently, Briggs et al. (2020) mentioned that fragmentation of particles into smaller slowly sinking particles by zooplankton could play an important role in supplying organic carbon to balance the carbon demand by bacteria in the mesopelagic zone. Additional studies are needed to look at the role of zooplankton in mesopelagic waters and to determine particle size and composition in the Red Sea.

4.8. Red Sea Waters Versus Other Oceanic Regions

Our mean transfer efficiency at 100-m depth below z_p (T_{100}) and remineralization exponent b were significantly different from values reported in the literature for different oceanic regions (Figures 10a and 10b). T_{100} was lower than other values reported in some of the oceanic regions of the global ocean (Figure 10b). Consistently, b was higher than those reported in different environments, even in other tropical and oligotrophic ecosystems (Figure 10a). The POC flux just below the productive layer (E_{z_p}) was lower than those reported in other areas of the global ocean except for the eastern part of the Mediterranean Sea (Figure 10c). Recent studies showed that most of the biomass of zooplankton in the Red Sea is mainly found in the upper layer of the water column (0–100 m) due to the presence of low oxygenated waters below 100 m (Karati et al., 2019). The scenario of low abundance of mesozooplankton in Red Sea waters may explain these differences. We can assume that most of the particles within the productive layer are fragmented into smaller size by zooplankton and are then degraded by bacteria in the mesopelagic zone. Regarding the TOC remineralization rates, our values agree well with those reported for some oceanic regions of the global ocean (Figure 10d). However, no clear information regarding the temporal and spatial variability of the $\Delta C{:}\Delta O_2$ Redfield ratios in the Red Sea is known. Uncertainties should be considered when using conversion factors to estimate TOC based on the Redfield ratio. It is known that temporal

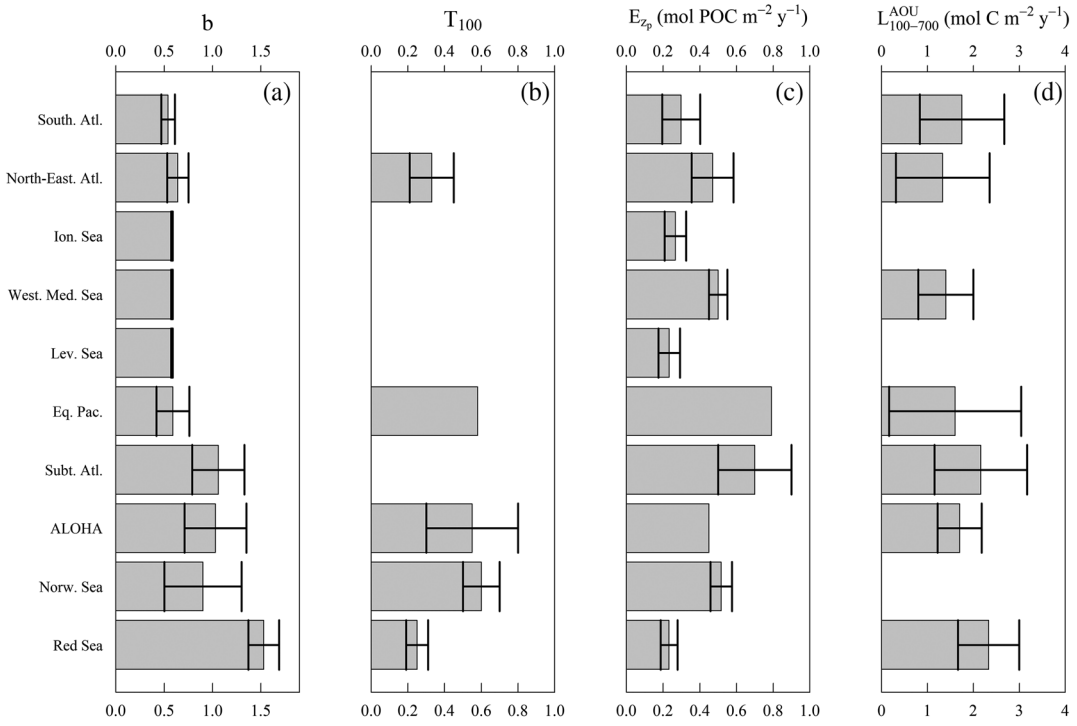

Figure 10. Comparison of flux attenuation coefficient (b), the net POC flux just below the productive layer (E_{z_p}), the transfer efficiency at 100-m depth (T_{100}), and the net TOC loss rates ($L^{AOU}_{z_i}$) with literature values for various oceanic regions. Error bars represent one standard deviation. Note: b (Guidi et al., 2015; Henson et al., 2012; Marsay et al., 2015; Martin et al., 1987), T_{100} (Buesseler & Boyd, 2009; Dall'Olmo & Mork, 2014; Devries & Weber., 2017; Honjo et al., 2008; Weber et al., 2016), E_{z_p} (Boyd & Newton, 1995; Buesseler et al., 2007; Buesseler & Boyd, 2009; Dall'Olmo & Mork, 2014; Devries & Weber., 2017; Durkin et al., 2015; Emerson, 2014; Giering et al., 2014; Guieu et al., 2005; Guieu et al., 2014; Henson et al., 2012; Honjo et al., 2008; Lohrenz et al., 1992; Marsay et al., 2015; Moutin & Raimbault, 2002; Shih et al., 2015; Weber et al., 2016), and $L^{AOU}_{100-700}$ (Abell et al., 2000; Aristegui et al., 2003; Calleja et al., 2019; Carlson et al., 1994; DeVries & Weber, 2017; Doval & Hansell, 2000; Feely et al., 2004; Hansell & Carlson, 2001; Karstensen et al., 2008; Lefèvre et al., 1996; Martz et al., 2008; Nagata et al., 2000; Roshan & DeVries, 2017).

and regional differences in $\Delta C{:}\Delta O_2$ Redfield ratio may appear depending on which biogeochemical processes predominate (Burd et al., 2010; Reinthaler et al., 2006). The common value 0.688 has been used to convert AOU into TOC here, which might not be appropriate of the Red sea and could result in higher or lower estimates of TOC consumption. Thus, while our estimates are within the range of those reported in other areas of the global ocean, they should be considered with caution. Future work should investigate quantitatively how these uncertainties affect our understanding of the carbon fluxes in the mesopelagic layer.

We also investigated the relationship between the median temperature within the upper layer of the water column (0–500 m) (where the remineralization of particles mainly occurs) using the data set from the World Ocean Atlas climatology (WOA13) and the Martin's curve exponent b for various regions of the global ocean (Figure 11a; Marsay et al., 2015). Both parameters were significantly correlated ($[b = 0.05\mathrm{T} + 0.25]$, $R^2 = 0.85$, $N = 7$, $p < 0.001$), suggesting that temperature may be used as a proxy to predict the effect of climate change on carbon fluxes in the Red Sea. However, we also obseved a strong correlation between organic carbon loss rates and oxygen (Figures 7 and 8), which suggests that temperature changes might mask variations in oxygen (Figure S8). Indeed, we also found a significant relationship between b and the median AOU ($[b = -0.01\mathrm{AOU} + 0.45]$, $R^2 = 0.90$, $N = 7$, $p < 0.001$, Figure 11b) as well as the median oxygen ($[b = -0.03\mathrm{O}_2 + 7]$, $R^2 = 0.90$, $N = 7$, $p < 0.001$, Figure 11c) using the data set from the World Ocean Atlas climatology (WOA09) within the upper layer of the water column (0–500 m) and for various regions of the global ocean. Oxygen is known to be a critical factor affecting growth rates of the heterotrophic communities

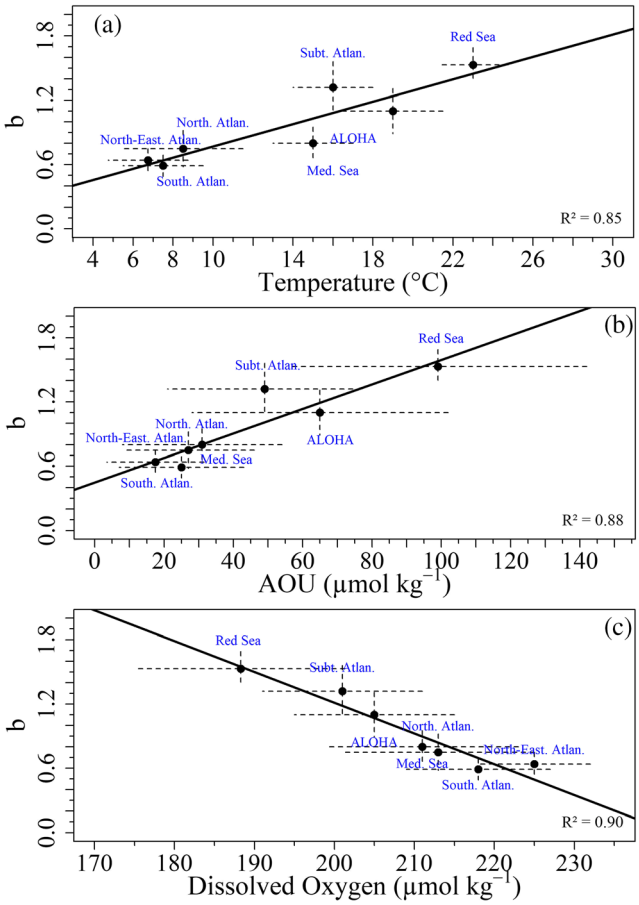

Figure 11. Flux attenuation coefficient, *b*, as a function of the median temperature (a), oxygen (b), and AOU (c) of the upper 500 m of the water column for various oceanic regions. Error bars represent the standard deviation.

and remineralization processes, and thus, the observed oxygen dependence of *b* may be as useful a parameter as the temperature dependence for future projections in the context of climate change. Interestingly, because oxygen concentrations depend strongly on temperature, oxygen might be used as a proxy for flux attenuation that combines both the effects of oxygen availability and temperature. Further studies to confirm this hypothesis are needed.

While it is known that POC remineralization varies with time and space in the oceans (Buesseler & Boyd, 2009), little is known about this variability and most global biogeochemical models use a constant $b = 0.86$ and a fixed remineralization rate (in depth and time) (0.025 d^{-1}) to estimate ocean carbon sequestration from sinking POC (DeVries & Weber, 2017; Dutkiewicz et al., 2005; Segschneider & Bendtsen, 2013). A constant *b* value and a fixed remineralization rate are clearly not representative of natural conditions and thus likely lead to uncertainties in predictions of global carbon sequestration. Our observed TOC remineralization rates (loss rates) converge with previous estimates using different approaches reported in the literature (Figure 10d). However, many of those depend on conversion parameters which may vary in time and space as well inducing high variability. Future work should investigate quantitatively how these uncertainties affect our understanding of the ocean carbon cycle.

5. Conclusion

In this study, we found that POC exported in the mesopelagic zone was rapidly degraded in a first stage and slowly in a second stage likely by heterotrophic organisms. We hypothesized that these differences in POC loss rates may depend on the palatability of the organic matter (from labile and nutritive at the start vs. recalcitrant and less palatable later). Regarding the TOC degradation (AOU-based), we found higher loss rates compared to POC loss rates, which are likely due to the consumption of dissolved organic carbon tracked by AOU and perhaps on the differences observed in the timing between POC and TOC loss.

We then observed that organic loss rates could be potentially expressed as a function of temperature and/or oxygen and thus could be used to predict their changes in response to climate change. We also showed a significant correlation between *b* values and the median upper 500 m water temperature and AOU with greater *b* values in warm waters where we observed high respiration processes by heterotrophs. Such regional variability in *b* showed that a uniform *b* value in the open ocean might not be necessarily appropriate to estimate or predict the feedback of ocean carbon remineralization on atmospheric carbon in the future as suggested by Marsay et al. (2015) and Weber et al. (2016). As we observed a rapid remineralization of the organic matter within the upper layer of the mesopelagic zone, further studies of the processes controlling the size and nature of the particles between 0 and 500-m depth are necessary to study the size and the nature of the particles in such environment. Currently, BGC-Argo floats do not provide this information. The next configuration of the BGC-Argo floats will enable a better understanding of the nature of the particles and the role of the heterotrophic organisms (zooplankton and bacteria) with a particular focus on the upper mesopelagic layer (Boyd et al., 2019). We also found that the sum of fast and slow POC losses led to a balanced budget for the small slowly sinking particles in the mesopelagic zone. The contribution of these particles could be a supplementary carbon source capable of balancing carbon budgets in the mesopelagic zone. Heterotrophic communities play an important role in regulating the efficiency of the BCP through controlling POC export by grazing, fragmenting, and degrading sinking particles in the global ocean. An outstanding scientific challenge is to understand the role of the heterotrophic communities in the mesopelagic zone. This will be possible with the development of new sensors on autonomous platforms (Boyd et al., 2019).

Data Availability Statement

The data presented here are freely available by the International Argo Program and the national programs that contribute to it (http://argo.jcommops.org).

Acknowledgments

The authors express their gratitude to the scientists, officers, and crews of the research vessel Thuwal for logistical support and assistance onboard during the deployment of the BGC-Argo float. U. Langner is cordially thanked for plotting the map of the Red Sea and L. Legendre, L. Prieur, Peter Brewer, and Edward Peltzer for their advices and discussions on the results presented here and for reading the manuscript. This study is funded by the King Abdullah University of Science and Technology (KAUST), Kingdom of Saudi Arabia. The collection of the data was funded by a European Research Council Advanced grant (remOcean, agreement no. 246577) while final writing was funded by a European Research Council Advanced grant (REFINE, agreement no. 834177).

References

Abell, J., Emerson, S., & Renaud, P. (2000). Distributions of TOP, TON and TOC in the North Pacific subtropical gyre: Implications for nutrient supply in the surface ocean and remineralization in the upper thermocline. *Journal of Marine Research*, *58*(2), 203–222. https://doi.org/10.1357/002224000321511142

Anderson, L. A., & Sarmiento, J. L. (1994). Redfield ratios of remineralization determined by nutrient data-analysis. *Global Biogeochemical Cycles*, *8*(1), 65–80. https://doi.org/10.1029/93GB03318

Anderson, T. R., & Ryabchenko, V. (2009). Carbon cycling in the mesopelagic zone of the central Arabian Sea: Results from a simple model. In J. D. Wiggert et al. (Eds.), *Indian Ocean: Biogeochemical processes and ecological variability*, *Geophysical Monograph Series* (Vol. 185, pp. 287–304). Washington, DC: American Geophysical Union. https://doi.org/10.1029/2007GM000686

Aristegui, J., Agusti, S., & Duarte, C. M. (2003). Respiration in the dark ocean. *Geophysical Research Letters*, *30*(2), 1041. https://doi.org/10.1029/2002GL016227

Arrhenius, S. (1889). On the reaction velocity of the inversion of cane sugar by acids, "Zeitschrift für physikalische Chemie" , 4, 226ff.

Baltar, F., Aristegui, J., Gasol, J. M., Sintes, E., & Herndl, G. J. (2009). Evidence of prokaryotic metabolism on suspended particulate organic matter in the dark waters of the subtropical North Atlantic. *Limnology and Oceanography*, *54*(1), 182–193. https://doi.org/10.4319/lo.2009.54.1.0182

Boss, E., & Pegau, W. S. (2001). Relationship of light scattering at an angle in the backward direction to the backscattering coefficient. *Applied Optics*, *40*(30), 5503–5507. https://doi.org/10.1364/ao.40.005503

Boyd, P., & Newton, P. (1995). Evidence of the potential influence of planktonic community structure on the interannual variability of particulate organic carbon flux. *Deep-Sea Research Part I-Oceanographic Research Papers*, *42*(5), 619–639. https://doi.org/10.1016/0967-0637(95)00017-z

Boyd, P. W., Claustre, H., Levy, M., Siegel, D. A., & Weber, T. (2019). Multi-faceted particle pumps drive carbon sequestration in the ocean. *Nature*, *568*, 327–335. https://doi.org/10.1038/s41586-019-1098-2

Breitburg, D., Levin, L. A., Oschlies, A., Grégoire, M., Chavez, F. P., Conley, D. J., et al. (2018). Declining oxygen in the global ocean and coastal waters. *Science*, *359*, eaam7240. https://doi.org/10.1126/science.aam7240

Brewer, P. G., & Peltzer, E. T. (2017). Depth perception: The need to report ocean biogeochemical rates as functions of temperature, not depth. *Philosophical Transactions of the Royal Society a-Mathematical Physical and Engineering Sciences*, *375*, 20160319. https://doi.org/10.1098/rsta.2016.0319

Briggs, N., Dall'Olmo, G., & Claustre, H. (2020). Major role of particle fragmentation in regulating biological sequestration of CO_2 by the oceans. *Science*, *367*, 791–793. https://doi.org/10.1126/science.aay1790

Briggs, N., Perry, M. J., Cetinic, I., Lee, C., D'Asaro, E., Gray, A. M., & Rehm, E. (2011). High-resolution observations of aggregate flux during a sub-polar North Atlantic spring bloom. *Deep-Sea Research Part I-Oceanographic Research Papers*, *58*(10), 1031–1039. https://doi.org/10.1016/j.dsr.2011.07.007

Buesseler, K. O., Antia, A. N., Chen, M., Fowler, S. W., Gardner, W. D., Gustafsson, O., et al. (2007). An assessment of the use of sediment traps for estimating upper ocean particle fluxes. *Journal of Marine Research*, *65*(3), 345–416. https://doi.org/10.1357/002224007781567621

Buesseler, K. O., & Boyd, P. W. (2009). Shedding light on processes that control particle export and flux attenuation in the twilight zone of the open ocean. *Limnology and Oceanography*, *54*(4), 1210–1232. https://doi.org/10.4319/lo.2009.54.4.1210

Buesseler, K. O., Boyd, P. W., Black, E. E., & Siegel, D. A. (2020). Metrics that matter for assessing the ocean biological carbon pump. *Proceedings of the National Academy of Sciences*, *117*, 9679–9687. https://doi.org/10.1073/pnas.1918114117

Burd, A. B., Hansell, D. A., Steinberg, D. K., Anderson, T. R., Arístegui, J., Baltar, F., et al. (2010). Assessing the apparent imbalance between geochemical and biochemical indicators of meso- and bathypelagic biological activity: What the @$#! is wrong with present calculations of carbon budgets? *Deep-Sea Research Part Ii-Topical Studies in Oceanography*, *57*(16), 1557–1571. https://doi.org/10.1016/j.dsr2.2010.02.022

Burd, A. B., & Jackson, G. A. (2009). Particle aggregation. *Annual Review of Marine Science*, *1*(1), 65–90. https://doi.org/10.1146/annurev.marine.010908.163904

Calleja, M. L., Al-Otaibi, N., & Moran, X. A. G. (2019). Dissolved organic carbon contribution to oxygen respiration in the central Red Sea. *Scientific Reports*, *9*, 4690. https://doi.org/10.1038/s41598-019-40753-w

Calleja, M. L., Ansari, M. I., Rostad, A., Silva, L., Kaartvedt, S., Irigoien, X., & Moran, X. A. G. (2018). The mesopelagic scattering layer: A hotspot for heterotrophic prokaryotes in the Red Sea twilight zone. *Frontiers in Marine Science*, *5*, 259. https://doi.org/10.3389/fmars.2018.00259

Carlson, C. A., Ducklow, H. W., & Michaels, A. F. (1994). Annual flux of dissolved organic carbon from the euphotic zone in the Northwestern Sargasso Sea. *Nature*, *371*(6496), 405–408. https://doi.org/10.1038/371405a0

Cavan, E. L., Trimmer, M., Shelley, F., & Sanders, R. (2017). Remineralization of particulate organic carbon in an ocean oxygen minimum zone. *Nature Communications*, *8*, 14847. https://doi.org/10.1038/ncomms14847

Cetinic, I., Perry, M. J., Briggs, N. T., Kallin, E., D'Asaro, E. A., & Lee, C. M. (2012). Particulate organic carbon and inherent optical properties during 2008 North Atlantic Bloom Experiment. *Journal of Geophysical Research*, *117*, C06028. https://doi.org/10.1029/2011JC007771

Chaidez, V., Dreano, D., Agusti, S., Duarte, C. M., & Hoteit, I. (2017). Decadal trends in Red Sea maximum surface temperature. *Scientific Reports*, *7*, 8144. https://doi.org/10.1038/s41598-017-08146-z

Dall'Olmo, G., & Mork, K. A. (2014). Carbon export by small particles in the Norwegian Sea. *Geophysical Research Letters*, *41*, 2921–2927. https://doi.org/10.1002/2014GL059244

Davidson, E. A., & Janssens, I. A. (2006). Temperature sensitivity of soil carbon decomposition and feedbacks to climate change. *Nature*, *440*(7081), 165–173. https://doi.org/10.1038/nature04514

Davidson, E. A., Trumbore, S. E., & Amundson, R. (2000). Biogeochemistry—Soil warming and organic carbon content. *Nature*, *408*(6814), 789–790. https://doi.org/10.1038/35048672

de Boyer Montegut, C., Madec, G., Fischer, A. S., Lazar, A., & Iudicone, D. (2004). Mixed layer depth over the global ocean: An examination of profile data and a profile-based climatology. *Journal of Geophysical Research*, *109*, C12003. https://doi.org/10.1029/2004JC002378

DeVries, T., & Weber, T. (2017). The export and fate of organic matter in the ocean: New constraints from combining satellite and oceanographic tracer observations. *Global Biogeochemical Cycles*, *31*, 535–555. https://doi.org/10.1002/2016GB005551

Doval, M. D., & Hansell, D. A. (2000). Organic carbon and apparent oxygen utilization in the western South Pacific and the central Indian oceans. *Marine Chemistry*, *68*(3), 249–264. https://doi.org/10.1016/s0304-4203(99)00081-x

Durkin, C. A., Estapa, M. L., & Buesseler, K. O. (2015). Observations of carbon export by small sinking particles in the upper mesopelagic. *Marine Chemistry*, *175*, 72–81. https://doi.org/10.1016/j.marchem.2015.02.011

Dutkiewicz, S., Follows, M. J., & Parekh, P. (2005). Interactions of the iron and phosphorus cycles: A three-dimensional model study. *Global Biogeochemical Cycles*, *19*, GB1021. https://doi.org/10.1029/2004gb002342

Dypvik, E., & Kaartvedt, S. (2013). Vertical migration and diel feeding periodicity of the skinnycheek lanternfish (*Benthosema pterotum*) in the Red Sea. *Deep-Sea Research Part I-Oceanographic Research Papers*, *72*, 9–16. https://doi.org/10.1016/j.dsr.2012.10.012

Emerson, S. (2014). Annual net community production and the biological carbon flux in the ocean. *Global Biogeochemical Cycles*, *28*, 14–28. https://doi.org/10.1002/2013GB004680

Estapa, M., Durkin, C., Buesseler, K., Johnson, R., & Feen, M. (2017). Carbon flux from bio-optical profiling floats: Calibrating transmissometers for use as optical sediment traps. *Deep-Sea Research Part I-Oceanographic Research Papers*, *120*, 100–111. https://doi.org/10.1016/j.dsr.2016.12.003

Estapa, M. L., Feen, M. L., & Breves, E. (2019). Direct observations of biological carbon export from profiling rituals in the subtropical North Atlantic. *Global Biogeochemical Cycles*, *33*, 282–300. https://doi.org/10.1029/2018GB006098

Feely, R. A., Sabine, C. L., Schlitzer, R., Bullister, J. L., Mecking, S., & Greeley, D. (2004). Oxygen utilization and organic carbon remineralization in the upper water column of the Pacific Ocean. *Journal of Oceanography*, *60*(1), 45–52. https://doi.org/10.1023/B:JOCE.0000038317.01279.aa

Flament, P. (2002). A state variable for characterizing water masses and their diffusive stability: Spiciness. *Progress in Oceanography*, *54*(1–4), 493–501. https://doi.org/10.1016/s0079-6611(02)00065-4

Garcia, H. E., & Gordon, L. I. (1992). Oxygen solubility in seawater—Better fitting equations. *Limnology and Oceanography*, *37*(6), 1307–1312. https://doi.org/10.4319/lo.1992.37.6.1307

Giering, S. L. C., Sanders, R., Lampitt, R. S., Anderson, T. R., Tamburini, C., Boutrif, M., et al. (2014). Reconciliation of the carbon budget in the ocean's twilight zone. *Nature*, *507*, 480–483. https://doi.org/10.1038/nature13123

Gittings, J. A., Raitsos, D. E., Kheireddine, M., Racault, M. F., Claustre, H., & Hoteit, I. (2019). Evaluating tropical phytoplankton phenology metrics using contemporary tools. *Scientific Reports*, *9*, 674. https://doi.org/10.1038/s41598-018-37370-4

Gittings, J. A., Raitsos, D. E., Krokos, G., & Hoteit, I. (2018). Impacts of warming on phytoplankton abundance and phenology in a typical tropical marine ecosystem. *Scientific Reports*, *8*, 2240. https://doi.org/10.1038/s41598-018-20560-5

Goutx, M., Wakeham, S. G., Lee, C., Duflos, M., Guigue, C., Liu, Z. F., et al. (2007). Composition and degradation of marine particles with different settling velocities in the northwestern Mediterranean Sea. *Limnology and Oceanography*, *52*(4), 1645–1664. https://doi.org/10.4319/lo.2007.52.4.1645

Guidi, L., Legendre, L., Reygondeau, G., Uitz, J., Stemmann, L., & Henson, S. A. (2015). A new look at ocean carbon remineralization for estimating deepwater sequestration. *Global Biogeochemical Cycles*, *29*, 1044–1059. https://doi.org/10.1002/2014GB005063

Guieu, C., Ridame, C., Pulido-Villena, E., Bressac, M., Desboeufs, K., & Dulac, F. (2014). Impact of dust deposition on carbon budget: A tentative assessment from a mesocosm approach. *Biogeosciences*, *11*, 5621–5635. https://doi.org/10.5194/bg-11-5621-2014

Guieu, C., Roy-Barman, M., Leblond, N., Jeandel, C., Souhaut, M., Le Cann, B., et al. (2005). Vertical particle flux in the northeast Atlantic Ocean (POMME experiment). *Journal of Geophysical Research*, *110*, C07S18. https://doi.org/10.1029/2004JC002672

Hansell, D. A., & Carlson, C. A. (2001). Biogeochemistry of total organic carbon and nitrogen in the Sargasso Sea: Control by convective overturn. *Deep-Sea Research Part Ii-Topical Studies in Oceanography*, *48*(8–9), 1649–1667. https://doi.org/10.1016/s0967-0645(00)00153-3

Henson, S., Lampitt, R., & Johns, D. (2012). Variability in phytoplankton community structure in response to the North Atlantic oscillation and implications for organic carbon flux. *Limnology and Oceanography*, *57*(6), 1591–1601. https://doi.org/10.4319/lo.2012.57.6.1591

Herndl, G. J., & Reinthaler, T. (2013). Microbial control of the dark end of the biological pump. *Nature Geoscience*, *6*, 718–724. https://doi.org/10.1038/ngeo1921

Honjo, S., Eglinton, T., Taylor, C., Ulmer, K., Sievert, S., Bracher, A., et al. (2014). Understanding the role of the biological pump in the global carbon cycle: An imperative for ocean science. *Oceanography*, *27*, 10–16. https://doi.org/10.5670/oceanog.2014.78

Honjo, S., Manganini, S. J., Krishfield, R. A., & Francois, R. (2008). Particulate organic carbon fluxes to the ocean interior and factors controlling the biological pump: A synthesis of global sediment trap programs since 1983. *Progress in Oceanography*, *76*(3), 217–285. https://doi.org/10.1016/j.pocean.2007.11.003

Karati, K. K., Al-Aidaroos, A. M., Devassy, R. P., El-Sherbiny, M. M., Jones, B. H., Sommer, U., & Kurten, B. (2019). Ecohydrographic control on the community structure and vertical distribution of pelagic Chaetognatha in the Red Sea. *Marine Biology*, *166*, 30. https://doi.org/10.1007/s00227-019-3472-x

Karstensen, J., Stramma, L., & Visbeck, M. (2008). Oxygen minimum zones in the eastern tropical Atlantic and Pacific oceans. *Progress in Oceanography*, *77*(4), 331–350. https://doi.org/10.1016/j.pocean.2007.05.009

Kheireddine, M., Ouhssain, M., Claustre, H., Uitz, J., Gentili, B., & Jones, B. H. (2017). Assessing pigment-based phytoplankton community distributions in the Red Sea. *Frontiers in Marine Science*, *4*, 132. https://doi.org/10.3389/fmars.2017.00132

Kheireddine, M., Ouhssain, M., Organelli, E., Bricaud, A., & Jones, B. H. (2018). Light absorption by suspended particles in the Red Sea: Effect of phytoplankton community size structure and pigment composition. *Journal of Geophysical Research: Oceans*, *123*, 902–921. https://doi.org/10.1002/2017JC013279

Kwon, E. Y., Primeau, F., & Sarmiento, J. L. (2009). The impact of remineralization depth on the air-sea carbon balance. *Nature Geoscience*, *2*(9), 630–635. https://doi.org/10.1038/ngeo612

Laufkotter, C., John, J. G., Stock, C. A., & Dunne, J. P. (2017). Temperature and oxygen dependence of the remineralization of organic matter. *Global Biogeochemical Cycles*, *31*, 1038–1050. https://doi.org/10.1002/2017GB005643

Laufkotter, C., Vogt, M., Gruber, N., Aumont, O., Bopp, L., Doney, S. C., et al. (2016). Projected decreases in future marine export production: The role of the carbon flux through the upper ocean ecosystem. *Biogeosciences*, *13*, 4023–4047. https://doi.org/10.5194/bg-13-4023-2016

Le Moigne, F. A. C., Cisternas-Novoa, C., Piontek, J., Massmig, M., & Engel, A. (2017). On the effect of low oxygen concentrations on bacterial degradation of sinking particles. *Scientific Reports*, *7*, 16722. https://doi.org/10.1038/s41598-017-16903-3

Lefèvre, D., Denis, M., Lambert, C. E., & Miquel, J. C. (1996). Is DOC the main source of organic matter remineralization in the ocean water column? *Journal of Marine Systems*, *7*(2–4), 281–291. https://doi.org/10.1016/0924-7963(95)00003-8

Llort, J., Langlais, C., Matear, R., Moreau, S., Lenton, A., & Strutton, P. G. (2018). Evaluating Southern Ocean carbon eddy-pump from biogeochemical-Argo floats. *Journal of Geophysical Research: Oceans*, *123*, 971–984. https://doi.org/10.1002/2017JC012861

Lohrenz, S. E., Knauer, G. A., Asper, V. L., Tuel, M., Michaels, A. F., & Knap, A. H. (1992). Seasonal variability in primary production and particle flux in the Northwestern Sargasso Sea—United-States JGOFS Bermuda Atlantic time series study. *Deep-Sea Research Part a-Oceanographic Research Papers*, *39*(7-8A), 1373–1391. https://doi.org/10.1016/0198-0149(92)90074-4

Lopez-Urrutia, A., San Martin, E., Harris, R. P., & Irigoien, X. (2006). Scaling the metabolic balance of the oceans. *Proceedings of the National Academy of Sciences of the United States of America*, *103*(23), 8739–8744. https://doi.org/10.1073/pnas.0601137103

Lutz, M. J., Caldeira, K., Dunbar, R. B., & Behrenfeld, M. J. (2007). Seasonal rhythms of net primary production and particulate organic carbon flux to depth describe the efficiency of biological pump in the global ocean. *Journal of Geophysical Research*, *112*, C10011. https://doi.org/10.1029/2006JC003706

Marsay, C. M., Sanders, R. J., Henson, S. A., Pabortsava, K., Achterberg, E. P., & Lampitt, R. S. (2015). Attenuation of sinking particulate organic carbon flux through the mesopelagic ocean. *Proceedings of the National Academy of Sciences of the United States of America*, *112*, 1089–1094. https://doi.org/10.1073/pnas.1415311112

Marshall, J., Adcroft, A., Hill, C., Perelman, L., & Heisey, C. (1997). A finite-volume, incompressible Navier Stokes model for studies of the ocean on parallel computers. *Journal of Geophysical Research*, *102*(C3), 5753–5766. https://doi.org/10.1029/96JC02775

Martin, J. H., Knauer, G. A., Karl, D., & Broenkow, W. W. (1987). VERTEX: Carbon cycling in the northeast Pacific. *Deep Sea Research, Part I*, *34*(2), 267–285. https://doi.org/10.1016/0198-0149(87)90086-0

Martinez-Garcia, A., Sigman, D. M., Ren, H. J., Anderson, R. F., Straub, M., Hodell, D. A., et al. (2014). Iron fertilization of the subantarctic ocean during the last ice age. *Science*, *343*, 1347–1350. https://doi.org/10.1126/science.1246848

Martz, T. R., Johnson, K. S., & Riser, S. C. (2008). Ocean metabolism observed with oxygen sensors on profiling floats in the South Pacific. *Limnology and Oceanography*, *53*(5part2), 2094–2111. https://doi.org/10.4319/lo.2008.53.5_part_2.2094

Morel, A., & Berthon, J. F. (1989). Surface pigment, algal biomass profiles, and potential production of the euphotic layer—Relationships reinvestigated in view of remote sensing applications. *Limnology and Oceanography*, *34*(8), 1545–1562. https://doi.org/10.4319/lo.1989.34.8.1545

Moutin, T., & Raimbault, P. (2002). Primary production, carbon export and nutrients availability in western and eastern Mediterranean Sea in early summer 1996 (MINOS cruise). *Journal of Marine Systems*, *33-34*, 273–288. https://doi.org/10.1016/s0924-7963(02)00062-3

Nagata, T., Fukuda, H., Fukuda, R., & Koike, I. (2000). Bacterioplankton distribution and production in deep Pacific waters: Large-scale geographic variations and possible coupling with sinking particle fluxes. *Limnology and Oceanography*, *45*(2), 426–435. https://doi.org/10.4319/lo.2000.45.2.0426

Organelli, E., Barbieux, M., Claustre, H., Schmechtig, C., Poteau, A., Bricaud, A., et al. (2017). Two databases derived from BGC-Argo float measurements for marine biogeochemical and bio-optical applications. *Earth System Science Data*, *9*, 861–880. https://doi.org/10.5194/essd-9-861-2017

Organelli, E., Claustre, H., Bricaud, A., Schmechtig, C., Poteau, A., Xing, X. G., et al. (2016). A novel near-real-time quality-control procedure for radiometric profiles measured by bio-Argo floats: Protocols and performances. *Journal of Atmospheric and Oceanic Technology*, *33*, 937–951. https://doi.org/10.1175/jtech-d-15-0193.1

Organelli, E., Dall'Olmo, G., Brewin, R. J. W., Tarran, G. A., Boss, E., & Bricaud, A. (2018). The open-ocean missing backscattering is in the structural complexity of particles. *Nature Communications*, *9*, 5439. https://doi.org/10.1038/s41467-018-07814-6

Paris, C. B., Helgers, J., van Sebille, E., & Srinivasan, A. (2013). Connectivity modeling system: A probabilistic modeling tool for the multi-scale tracking of biotic and abiotic variability in the ocean. *Environmental Modelling & Software*, *42*, 47–54. https://doi.org/10.1016/j.envsoft.2012.12.006

Paulmier, A., Kriest, I., & Oschlies, A. (2009). Stoichiometries of remineralisation and denitrification in global biogeochemical ocean models. *Biogeosciences*, *6*(5), 923–935. https://doi.org/10.5194/bg-6-923-2009

Puigcorbe, V., Roca-Marti, M., Masque, P., Benitez-Nelson, C., van der Loeff, M. R., Bracher, A., & Moreau, S. (2017). Latitudinal distributions of particulate carbon export across the North Western Atlantic Ocean. *Deep-Sea Research Part I-Oceanographic Research Papers*, *129*, 116–130. https://doi.org/10.1016/j.dsr.2017.08.016

Rasse, R., Dall'Olmo, G., Graff, J., Westberry, T. K., van Dongen-Vogels, V., & Behrenfeld, M. J. (2017). Evaluating optical proxies of particulate organic carbon across the surface Atlantic Ocean. *Frontiers in Marine Science*, *4*, 367. https://doi.org/10.3389/fmars.2017.00367

Reinthaler, T., van Aken, H., Veth, C., Aristegui, J., Robinson, C., Williams, P., et al. (2006). Prokaryotic respiration and production in the meso- and bathypelagic realm of the eastern and western North Atlantic basin. *Limnology and Oceanography*, *51*(3), 1262–1273. https://doi.org/10.4319/lo.2006.51.3.1262

Robinson, C. (2019). Microbial respiration, the engine of ocean deoxygenation. *Frontiers in Marine Science*, *5*, 533. https://doi.org/10.3389/fmars.2018.00533

Robinson, C., Steinberg, D. K., Anderson, T. R., Arístegui, J., Carlson, C. A., Frost, J. R., et al. (2010). Mesopelagic zone ecology and biogeochemistry—A synthesis. *Deep-Sea Research Part Ii-Topical Studies in Oceanography*, *57*(16), 1504–1518. https://doi.org/10.1016/j.dsr2.2010.02.018

Roder, C., Berumen, M. L., Bouwmeester, J., Papathanassiou, E., Al-Suwailem, A., & Voolstra, C. R. (2013). First biological measurements of deep-sea corals from the Red Sea. *Scientific Reports*, *3*, 2802. https://doi.org/10.1038/srep02802

Roesler, C., Uitz, J., Claustre, H., Boss, E., Xing, X., Organelli, E., et al. (2017). Recommendations for obtaining unbiased chlorophyll estimates from in situ chlorophyll fluorometers: A global analysis of WET Labs ECO sensors. *Limnology and Oceanography: Methods*, *15*, 572–585. https://doi.org/10.1002/lom3.10185

Roshan, S., & DeVries, T. (2017). Efficient dissolved organic carbon production and export in the oligotrophic ocean. *Nature Communications*, *8*, 2036. https://doi.org/10.1038/s41467-017-02227-3

Sarmento, H., Montoya, J. M., Vazquez-Dominguez, E., Vaque, D., & Gasol, J. M. (2010). Warming effects on marine microbial food web processes: How far can we go when it comes to predictions? *Philosophical Transactions of the Royal Society, B: Biological Sciences*, *365*(1549), 2137–2149. https://doi.org/10.1098/rstb.2010.0045

Schmechtig, C., Poteau, A., Claustre, H., D'Ortenzio, F., & Boss, E. (2015). Processing bio-Argo chlorophyll-a concentration at the DAC level, v1.0. https://doi.org/10.13155/39468

Schmechtig, C., Poteau, A., Claustre, H., D'Ortenzio, F., Dall'Olmo, G., & Boss, E. (2016). Processing bio-Argo particle backscattering at the DAC level, Argo. https://doi.org/10.13155/39459

Segschneider, J., & Bendtsen, J. (2013). Temperature-dependent remineralization in a warming ocean increases surface pCO(2) through changes in marine ecosystem composition. *Global Biogeochemical Cycles*, *27*, 1214–1225. https://doi.org/10.1002/2013GB004684

Sempere, R., Yoro, S. C., Van Wambeke, F., & Charriere, B. (2000). Microbial decomposition of large organic particles in the northwestern Mediterranean Sea: An experimental approach. *Marine Ecology Progress Series*, *198*, 61–72. https://doi.org/10.3354/meps198061

Shih, Y. Y., Hung, C. C., Gong, G. C., Chung, W. C., Wang, Y. H., Lee, I. H., et al. (2015). Enhanced particulate organic carbon export at eddy edges in the oligotrophic Western North Pacific Ocean. *PLoS ONE*, *10*, e0131538. https://doi.org/10.1371/journal.pone.0131538

Sofianos, S. S., & Johns, W. E. (2007). Observations of the summer Red Sea circulation. *Journal of Geophysical Research*, *112*, C06025. https://doi.org/10.1029/2006JC003886

Steinberg, D. K., Van Mooy, B. A. S., Buesseler, K. O., Boyd, P. W., Kobari, T., & Karl, D. M. (2008). Bacterial vs. zooplankton control of sinking particle flux in the ocean's twilight zone. *Limnology and Oceanography*, *53*(4), 1327–1338. https://doi.org/10.4319/lo.2008.53.4.1327

Stramma, L., Schmidtko, S., Levin, L. A., & Johnson, G. C. (2010). Ocean oxygen minima expansions and their biological impacts. *Deep-Sea Research Part I-Oceanographic Research Papers*, *57*(4), 587–595. https://doi.org/10.1016/j.dsr.2010.01.005

Stramski, D., Boss, E., Bogucki, D., & Voss, K. J. (2004). The role of seawater constituents in light backscattering in the ocean. *Progress in Oceanography*, *61*(1), 27–56. https://doi.org/10.1016/j.pocean.2004.07.001

Stramski, D., Reynolds, R. A., Babin, M., Kaczmarec, S., Lewis, M. R., Röttgers, R., et al. (2008). Relationships between the surface concentration of particulate organic carbon and optical properties in the eastern South Pacific and eastern Atlantic Oceans. *Biogeosciences*, *5*, 171–201. https://doi.org/10.5194/bg-5-171-2008

Sullivan, J., Twardowski, M., Zaneveld, J. R. V., & Moore, C. (2013). Measuring optical backscattering in water. In A. A. Kokhanovsky (Ed.), *Light scattering reviews 7: Radiative transfer and optical properties of atmosphere and underlying surface* (pp. 189–224). Berlin: Springer Praxis Books. https://doi.org/10.1007/978-3-642-21907-8_6

Takeshita, Y., Martz, T. R., Johnson, K. S., Plant, J. N., Gilbert, D., Riser, S. C., et al. (2013). A climatology-based quality control procedure for profiling float oxygen data. *Journal of Geophysical Research: Oceans*, *118*, 5640–5650. https://doi.org/10.1002/jgrc.20399

Thierry, V., Bittig, H. C., Gilbert, D., Kobayashi, T., Kanako, S., & Schmid, C. (2018). Processing Argo oxygen data at the DAC level, v2.3.1. https://doi.org/10.13155/39795

Thierry, V., Bittig, H. C. & The Argo-Bgc Team (2018). Argo quality control manual for dissolved oxygen concentration, v2.0. https://doi.org/10.13155/46542

Thomas, H. (2002). Remineralization ratios of carbon, nutrients, and oxygen in the North Atlantic Ocean: A field databased assessment. *Global Biogeochemical Cycles*, *16*(3), 1051. https://doi.org/10.1029/2001gb001452

Torfstein, A., Kienast, S. S., Yarden, B., Rivlin, A., Isaacs, S., & Shaked, Y. (2020). Bulk and export production fluxes in the Gulf of Aqaba, Northern Red Sea. *ACS Earth and Space Chemistry*, *4*, 1461–1479. https://doi.org/10.1021/acsearthspacechem.0c00079

Weber, T., Cram, J. A., Leung, S. W., DeVries, T., & Deutsch, C. (2016). Deep ocean nutrients imply large latitudinal variation in particle transfer efficiency. *Proceedings of the National Academy of Sciences of the United States of America*, *113*, 8606–8611. https://doi.org/10.1073/pnas.1604414113

Wong, A., Keeley, R., Carval, T., Tand the Argo Data Management Team (2015). Argo quality control manual for CTD and trajectory data, Version 3, 56 pp. https://doi.org/10.13155/33951

Xing, X. G., Briggs, N., Boss, E., & Claustre, H. (2018). Improved correction for non-photochemical quenching of in situ chlorophyll fluorescence based on a synchronous irradiance profile. *Optics Express*, *26*, 24,734–24,751. https://doi.org/10.1364/oe.26.024734

Yao, F. C., Hoteit, I., Pratt, L. J., Bower, A. S., Kohl, A., Gopalakrishnan, G., & Rivas, D. (2014a). Seasonal overturning circulation in the Red Sea: 2. Winter circulation. *Journal of Geophysical Research: Oceans*, *119*, 2263–2289. https://doi.org/10.1002/2013jc009331

Yao, F. C., Hoteit, I., Pratt, L. J., Bower, A. S., Zhai, P., Kohl, A., & Gopalakrishnan, G. (2014b). Seasonal overturning circulation in the Red Sea: 1. Model validation and summer circulation. *Journal of Geophysical Research: Oceans*, *119*, 2238–2262. https://doi.org/10.1002/2013jc009004

Zaneveld, R., Boss, E., & Barnard, A. (2001). Influence of surface waves on measured and modeled irradiance profiles. *Applied Optics*, *40*, 1442–1449. https://doi.org/10.1364/AO.40.001442

Zhang, X. D., Hu, L. B., & He, M. X. (2009). Scattering by pure seawater: Effect of salinity. *Optics Express*, *17*(7), 5698–5710. https://doi.org/10.1364/oe.17.005698